Master Thesis in Materials, Energy and Nanotechnology.

Brian Walela Wabende

A study of niobium-doped titanium dioxide as viable material for water photocatalysis.

DEPARTMENT OF PHYSICS

FACULTY OF MATHEMATICS AND NATURAL SCIENCES.

UNIVERSTITY OF OSLO.

August, 2013

Foreword.

The thesis represents a study that has been done as part of my masters study in Materials, Energy and Nanotechnology (MENA) at the University of Oslo. The study was done at the Centre for Material science and Nanotechnology (SMN) from august 2011 until august 2013.

I would like to thank my supervisors Truls E. Norby, Kingsley O. Iwu and Agnieszka G. Sobas for spending hours on informing me on how to think and proceed on hanling the subject matter.

I would like to thank God for giving me this opportunity, my family and friends for their support.

I would also like to thank my fellow colleagues at FERMiO and the rest in the Department for the assistance they have given me during my study.

University of Oslo, August 2013

Brian Elijah Walela Wabende.

Table of Contents

1. INTRODUCTION.

The use of hydrocarbon fossil fuels is proving to be an unsustainable source of energy. This is due to it producing pollutants which have a negative effect on the environment. The other reason is that the resources of these types of fuels are becoming depleted. This has led to research in renewable energy sources. Our main source of energy is the Sun. The Sun leads in the producion of energy from hydropower, wind energy, photovoltaics and concentrated solar power to mention but a few.

A problem with many types of solar-based energy sources such as wind, waves and photovolataics is that they produce electrical energy with varying intensity over the year, during the day with varying weather conditions and electricity cannot be easily stored.

Solutions to this problem of storage is the making of better batteries for storage of energy, or find an alternative means of energy storage like hydrogen.

Batteries have been developed to a great extent in the recent years. The problem that still plagues the batteries is the loss of charge while not being used.[1] This is in addition to the internal resistance of the battery. This leads to decrease in efficiency and loss of energy. A solution for this might be hydrogen as an energy storage material. Storing hydrogen as a gas is not energy efficient as a small amount of gas occupies a large volume. Liquefying the gas ends up using more energy. The nascent research in hydride proves to be a promising method of storing hydrogen. These materials have high hydrogen content per volume as compared to the aforementioned methods of storage.[2] This is why finding an easy way of getting an easy way of producing hydrogen is important as we get to harness energy from the sun.

The objective of this project is to study the direct production of hydrogen from water by the use of Niobium doped titania (Nb-doped TiO_2), which is an n-type semiconductor.

The goals of this project are to design and build a photoelectrochemical cell and study the photo-catalytic properties of Nb-TiO_2.

[1] http://en.wikipedia.org/wiki/Lithium-ion_battery#Advantages_and_disadvantages
[2] http://en.wikipedia.org/wiki/Hydrogen_storage

Project plan.

This project will consist of the following parts:

1. Synthesis and fabrication of nanostructured samples of Nb-TiO_2.
2. Characterisation of samples.
3. Design, fabrication and testing of photoelectrochemical cells for testing of individual electrodes.
4. Testing of the Nb-TiO_2 as a photoanode vs. Pt cathode.

Methodology.

1. Synthesis and fabrication of nanostructured samples of Nb-TiO_2.

The TiO_2 will be of nanosize, preferably between 10-20 nm. This will then be pressed into a cylinder with a circumference of 2 cm and a thickness of 1 mm. The compound can be synthesised by using both solid-state and sol-gel methods.

Nano sized particles of the compound are going to be used in the project. These can be made into thin films by using either of the two techniques: Pulsed Laser Deposition (PLD) and/or Spin Coating. In both cases you preserve the composition of the original compound.

2. Characterisation of samples.

The samples will be characterised using different characterisation techniques e.g. scanning electron microscopy, x-ray photoelectron spectroscopy, x-ray diffraction etc.

3. Design, fabrication and testing of photoelectrochemical cells for testing of individual electrodes.

The experiments will be carried out in the photoelectrochemical cell. It thereby needs an electrolyte supply source, gas outlets, a window to let in light, stage to mount the sample, electrodes, gas inlet, salt bridge and other outlets for any additional equipment. It would be preferable if the walls of the PEC absorbed UV light so as to minimize undesired effects. The

cell will be divided into two containers. One containing the photoanode, whilst the other one will have the cathode.

4. **Testing of the Nb-TiO_2 as a photoanode vs. Pt cathode.**

The Nb-TiO_2 samples will be used to make thin films. The thin films will be made on a conducting substrate. The thin films will then be put in the photoelectrochemical cell and connected to the Pt cathode via an external circuit.

2. THEORY.

Defect chemistry.

Most structures above 0 K contain defects, i.e. divergence from the ideal structure. This is due to the thermal energy gained by the atoms, leading to their migration. Defects give solid state materials some of their properties, e.g. diffusion, conductivity (electrical and thermal). Defect chemistry is the comprehensive study of different defects and how they can be applied in material science. Most of the literature in this section is taken from Kofstad's and Norby's book on defect chemistry. (footnote)

There are zero to three dimensional defects. In this paper the main defects that are considered are vacancies, interstitials, substitutions and grain boundaries. The first three are considered as zero dimensional or point defects. The last defect is a two dimensional defect. Electronic defects are also considered. This is the formation of an electron-hole pair.

Point defects.

Defects are represented by use of the Kröger-Vink notation. This notation gives information on the type of defect, the effective charge on the defect and the site at which the defect is located.

In niobium-doped titania the following point defects can be found:

Defects in Nb-TiO_2	**Kröger-Vink notation.**
Titanium vacancy	$v_{Ti}^{////}$
Oxygen vacancy	$v_O^{\bullet\bullet}$
Titanium interstitial	$Ti_i^{\bullet\bullet\bullet\bullet}$
Oxygen interstitial	$O_i^{//}$
Niobium substitution	$Nb_{Ti}^{\bullet}$
Hydrogen interstitial	$OH_O^{\bullet}$
Electron	$e^{/}$
Hole	$h^{\bullet}$

The formation of the above defects can be represented with equilibrium equations. The equations must obey three rules:

- Conservation of mass
- Conservation of charge
- Conservation of site ratio

Below are equations describing the formation of these defects.

This is the formation of a titanium vacancy.

$$O_{2_{(g)}} + 4e^{/} = v_{Ti}^{////} + 2O_O^x$$

This is the formation of an oxygen vacancy.

$$O_O^x = v_O^{\bullet\bullet} + 2e^{//} + \frac{1}{2}O_2$$

This is the formation of niobium substitution in titanium site.

$$Nb_2O_5 = 2Nb_{Ti}^{\bullet} + 4O_o^x + 2e^{/} + \frac{1}{2}O_2$$

This is the formation of hydrogen interstitial.

$$\frac{1}{2}H_2O + O_O^x = OH_O^{\bullet} + e^{/} + \frac{1}{4}O_2$$

This is the formation of an electron-hole pair.

$$0 = e^{/} + h^{\bullet}$$

Band theory.

Band theory is a theory used to explain the electronic behaviour of materials. It is a continuation of the molecular orbital theory, which suggests that molecular orbitals are formed by the linear

combination of atomic orbitals. (LCAO-MO) The continual addition of atoms leads to the formation of bands. At 0K materials have filled and unfilled bands. As the temperature increases the electrons gain energy and are excited to higher bands. This leads to partial filling of the unfilled bands.

In metals the highest filled band overlaps with the unfilled band and thereby electrons have empty states to migrate to with minimal energy (E < kT). This is why metals are conductors. In insulators there is a gap between the filled and empty bands and thereby require a high energy for excitation. This is the reason for them being non-conductors. In between are semi-conductors which have a lesser band gap than the insulators (<3.5 eV) and their electrons can be excited either thermally or by use of electromagnetic waves in the visible light region of the spectrum.

The filled band is called the valence band, while the unfilled band is called the conduction band. Electrons are excited by light or thermally from the valence band to the conduction band. In the conduction band the electron can migrate (abundance of empty states) and leading to the material being conductive.

The highest filled energy state is called the Fermi level. In an intrinsic semiconductor the value of the Fermi level is given by,

$$E_F = \frac{1}{2} E_G$$

This means that the Fermi level is half the value of the energy gap between the conduction band and the valence band.

When minuscule amounts of dopants are added to the material, new energy states are formed in the band gap of the material. If the dopant is a donor, the state is formed just below the conduction band, and if an acceptor, then the state is formed just above the valence band. The donor doped semiconductors are also known as n-type semiconductors, while the acceptor doped semiconductors are known as the p-type semiconductors. The difference between the new states and the bands is small enough to allow thermal excitation. The Fermi level of doped semiconductors are different to that of intrinsic semiconductors. The Fermi level can be found by using the following general equation:

$$E_F = \frac{1}{2}(E_{VB} + E_{CB}) + \frac{1}{2}\left(kT\ ln\frac{N^*_{VB}}{N^*_{CB}}\right)$$

where,

E_{VB} is valence band edge energy

E_{CB} is the conduction band energy

k is Boltzmann constant

T is absolute temperature

N^*_{VB} and N^*_{CB} are the effective densities (energy) of states of the valence band and conduction band respectively.

From the above formula it can be seen that when the semiconductor is intrinsic, then the second part of the equation is reduced to zero, since the density of states of electrons and holes in the conduction band and valence band respectively are equal. The general formula is thereby reduced to the Fermi level formula shown before. For the doped semiconductors, the Fermi level will be closer to the conduction band for n-type semiconductors, and conversely near the valence band for the p-type semiconductor. This is due to the variation of density of states in the two situations.

Photocatalysis

For one to understand photocatalysis, one must, in addition to band theory, understand the basic physical principle of photoelectric effect. This is understood by taking light as being a particle of energy, with a certain energy value, called a photon. When a photon reaches the material, it is either absorbed by electrons or it passes through the material without any interaction. After the photon is absorbed by the electron, the electron becomes excited and migrates to a higher energy level (allowed quantum states). For the photon absorption to occur, it must contain energy equal to or greater than the energy difference between the two energy levels (initial or ground state energy level to final or exited energy level). The promotion of the electron to a high energy state

leave the previously occupied low energy state empty. The empty state can be taken as being a positively charge particle (quasiparticle), hole, surrounded by negatively charges electrons. The creation of this charge pair (exciton) is necessary for photocatalysis. The electron is conducted away to the cathode where it will reduce one of the chemical species in the electrolyte. The hole on the other hand, will oxidise a chemical specie in the electrolyte.

In this investigation the hole oxidises water into hydrogen ion and a hydroxide ion is formed which eventually end up changing to oxygen gas. The hydrogen ion diffuses to the platinum cathode where it is reduced to hydrogen atom.

3. LITERATURE.

Undoped and doped titanium dioxide.

Titanium dioxide (TiO_2) has two common polymorphs: anatase and rutile crystal structures. Of the two, rutile is the most stable. Anatase transforms to rutile between 550 and 1000°C. This transformation may also be promoted by the presence of impurities as shown by Hanaor and Sorrell (Hanaor and Sorrell 2011).

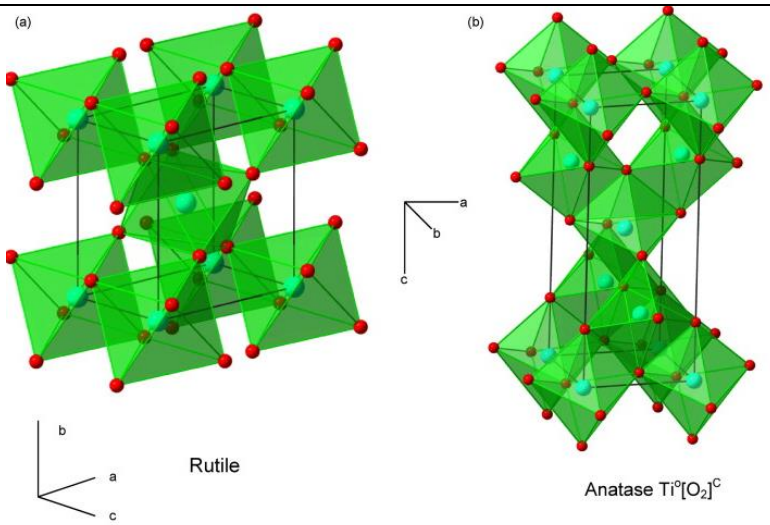

Figure 1: (a) Rutile and (b) anatase structures. Figure from Yang et. al.(Yang, Choi et al. 2009)

When a donor dopant, in this case niobium (Nb) is inserted into the structure, it loses an electron to the structure and becomes positively charged. Nb is a pentavalent element (Nb^{5+}), while Ti is tetravalent (Ti^{4+}) [3] and therefore Nb becomes $Nb^{\bullet}_{Ti}$.(Sheppard, Dittrich et al. 2012) The doping also introduces structural strain as the $Nb^{\bullet}_{Ti}$ is not the same size as Ti_{Ti}. This may lead to changes in configuration of energy states.(Depero, Sangaletti et al. 1998, Ok, Park et al. 2012)

[3] Grimes, C. A., Ranjan, S., Varghese, O. K. *Light, Water, Hydrogen: The Solar Generation of Hydrogen by Water Photoelectrolysis.* Springer Science+Business Media, LLC; 2008.

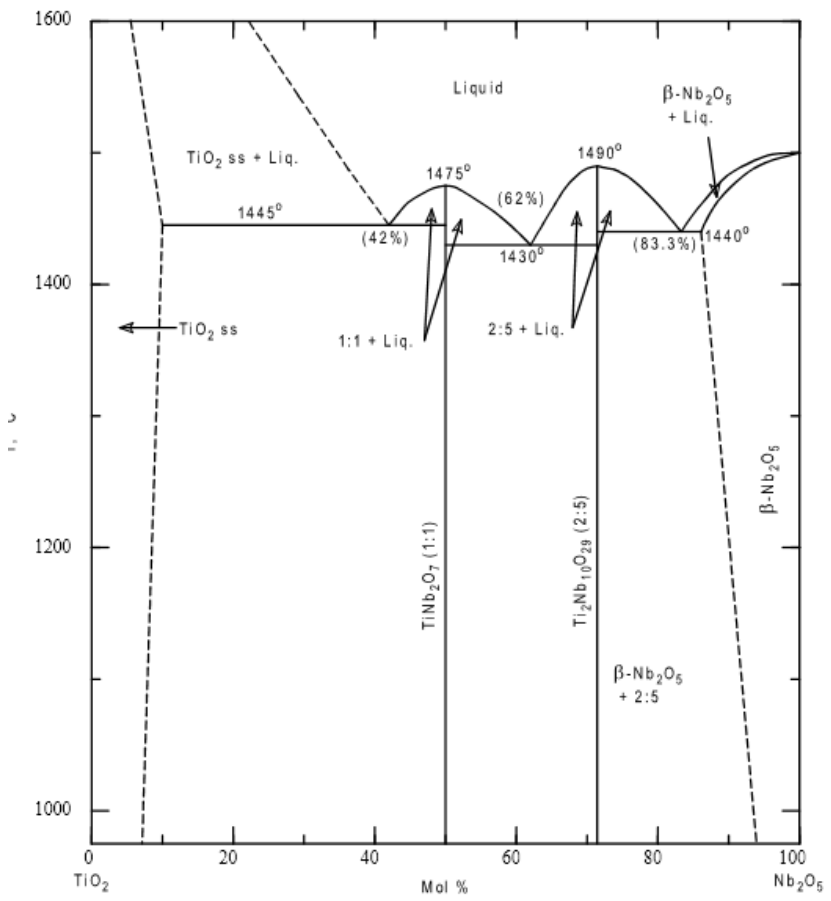

Figure 2: Phase diagram of titanium dioxide-niobium (V) oxide.[4]

The phase diagram in figure 2 shows the different compounds formed upon mixing TiO_2 and niobium (V) oxide (Nb_2O_5). It can be seen that the solubility limit of Nb_2O_5 in TiO_2 at 1400°C is approximately 8%. After this limit other phases start to form, like titanium niobate $TiNb_2O_7$. Even within the 8% limit there is segregation of Nb on the grain boundaries due to both kintecis and chemical equilibrium as affected by external entities such as oxygen partial pressure.(Sheppard, Dittrich et al. 2012, Sheppard 2013)

[4] Babich, T. G., Zagorodnyuk, A. V., Teterin, G. A., Khodos, M. Y., Zhirnova, A. P. Russ J Inorg Chem (Engl Transl). 1988;33(4):3.

Photocatalysis.

Photocatalysis was reported in the early part of the 20th centrury and it was in Japan that the earliest records of TiO_2 as a photocatalyst was recorded by Mashio et. al. TiO_2 is taken to be a promising photocatlyst, albeit its high band gap of about 3 eV. This means that doping is necessary in order to reduce the energy needed for photo-excitation. It is stable under most conditions, unlike e.g. iron oxide which has a smaller band gap, and that is why it is being investiagted.(Hashimoto, Irie et al. 2005, Kudo 2006, Ni, Leung et al. 2007)

TiO_2 is thereby manufactured into different nano-strucutures in order to reduce it's band gap and increase it's surface area for increased efficiency.(Ok, Park et al. 2012)

Depero, L. E., et al. (1998). "Niobium-titanium oxide powders obtained by laser-induced synthesis: Microstructure and structure evolution from diffraction data." Journal of Materials Research **13**(06): 1644-1649.

Hanaor, D. H. and C. Sorrell (2011). "Review of the anatase to rutile phase transformation." Journal of Materials Science **46**(4): 855-874.

Hashimoto, K., et al. (2005). "TiO~ 2 Photocatalysis: A Historical Overview and Future Prospects." JAPANESE JOURNAL OF APPLIED PHYSICS PART 1 REGULAR PAPERS SHORT NOTES AND REVIEW PAPERS **44**(12): 8269.

Kudo, A. (2006). "Development of photocatalyst materials for water splitting." International Journal of Hydrogen Energy **31**(2): 197-202.

Ni, M., et al. (2007). "A review and recent developments in photocatalytic water-splitting using for hydrogen production." Renewable and Sustainable Energy Reviews **11**(3): 401-425.

Ok, K.-C., et al. (2012). "Semiconducting behavior of niobium-doped titanium oxide in the amorphous state." Applied Physics Letters **100**(14): 142103-142103.

Sheppard, L. (2013). "Niobium Surface Segregation in Polycrystalline Niobium-Doped Titanium Dioxide." The Journal of Physical Chemistry C **117**(7): 3407-3413.

Sheppard, L. R., et al. (2012). "The Impact of Niobium Surface Segregation on Charge Separation in Niobium-Doped Titanium Dioxide." The Journal of Physical Chemistry C **116**(39): 20923-20929.

Yang, Z., et al. (2009). "Nanostructures and lithium electrochemical reactivity of lithium titanites and titanium oxides: A review." Journal of Power Sources **192**(2): 588-598.

4. EXPERIMENTAL

Sample Preparation

Solid-State method

There were three different samples of TiO_2 with different doping levels- 1%, 3% and 30% (Atomic percentages). The samples were prepared using solid state method. Titanium (IV) oxide, TiO_2, (Alfa Aesar TiO_2, rutile, 99.8% (metal basis), 0.9-1.6 micron APS Powder) and niobium (V) oxide, Nb_2O_5, (Alfa Aesar Nb_2O_5, 99.9% (metal basis)) were mixed together using ball milling method. Table 1 shows both the calculated and measured amount of powder of each compound used in making the different pellets. (Total mass of pellet was chosen to be 5 g.)

Compound	**1% Nb-doped TiO_2**	
	Calculated mass (g)	**Measured mass (g)**
Nb_2O_5	0.082739	0.0828
TiO_2	4.922242	4.9227
	3% Nb-doped TiO_2	
	Calculated mass (g)	**Measured mass (g)**
Nb_2O_5	0.245463	0.2457
TiO_2	4.769312	4.7734
	30% Nb-doped TiO_2	
	Calculated mass (g)	**Measured mass (g)**
Nb_2O_5	2.134958	2.1358
TiO_2	2.993547	2.9933

Table 1: Calculated and measured mass of pellet precoursors

Ball milling was done by putting the powder in the container with the balls and adding isopropanol to it, and milling the mixture for 1 hour at a revolution speed of 200 rpm (rotations/revoltutions per minute).

The sample was then filtered, dried, mixed with a binder and pressed into a pellet followed by sintering at 1400 °C for 6 hours. It was done using the following recipe found in Ingrid Nygård's thesis.[5]

$$RT \xrightarrow{150°C/h} 500°C \xrightarrow{200°C/h} 1300°C \xrightarrow{60°C/h} 1400°C \xrightarrow{6h\ dwell} 1400°C \xrightarrow{150°C/h} RT$$

The relative density of the pellets after sintering was calculated using the following formula:

$$\frac{\rho_{pellet}}{\rho_{rutile}} = \frac{m_{pellet}}{V_{pellet} \times 4.23\ g\ cm^{-3}}$$

The density of rutile is used as the reference density. This is done so, because most of the sample is made up of rutile and thereby the effect of the density of Nb_2O_5 will be insignificant. The relative densities of the pellets were found to be between 96-97%.

Pulsed-laser deposition (PLD)

In preparation for PLD, the pellets were polished using silicon carbide polishing papers. The papers used were numbered 500, 800, 1000 and 1200. The papers are made such that the lower the number the larger the size of silicon carbide grains. Below is a table showing the grit size of the aforementioned numbers.

Microgrits	**Average particle diameter (µm)**
500	30.2
800	6.5
1000	18.3
1200	2.5

Table 2:Table showing correlation between standard ANSI grit and grain size

The polished samples were used as targets for PLD thin films. The films were deposited on silicon wafers, silica glass and fluorine doped tin oxide glass (FTO-glass) substrates. The PLD machine (SURFACE systems+technology GmbH & Co. KG Pulsed Laser Deposition (PLD) systems) utilised a laser of wavelength 248 nm to sputter the target. The substrates were first

[5] Nygård, I.H.. Electrical characterisation of grain boundaries in donor doped TiO_2. Master of Science, University of Oslo, 2012.

cleaned using acetone, deionised water and isopropanol by sonication in an ultra-sound. Afterwards they were cleaned by blowing air on them and then mounted onto the sample holder. For the samples used in the solar simulator, part of the conducting FTO-glass was masked using aluminium foil, in order to provide an electrical contact to the Potentiostat. (Figure 1)

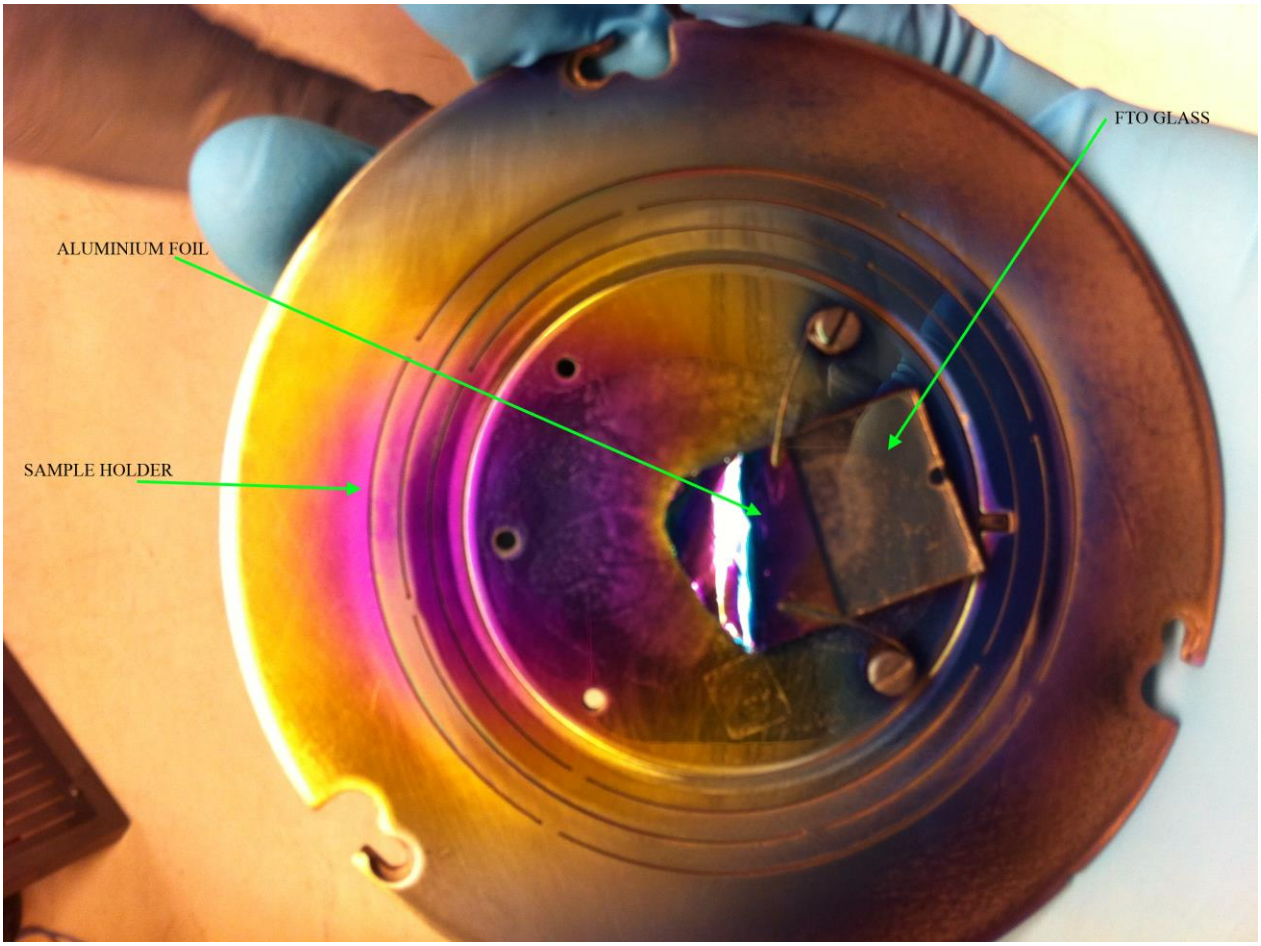

Figure 3: PLD sample holder with FTO sample glass on it

Before deposition, the chamber was evacuated to about 5×10^{-9} atm. This was done to remove the adsorbed gases on the chamber walls. The substrate was then heated up and the pressure increased to about 1×10^{-4} atm. This was done by using the inert gas argon. Thereafter laser ablation commenced. After laser ablation, the sample was then cooled and demounted from the machine. The substrate temperature for FTO-glass was 400°C, while the other mentioned substrates were heated up to 700°C.

Characterisation

Scanning electron microscopy (SEM)

The pellets' and the thin films' morphology, phases and chemical contents were examined using scanning electron microscopy. The microscope used is of the type *FEG-SEM Quanta 200F (FEI Company, USA).*

The microscope has two types of detectors for detecting secondary electrons, (which give information about the morphology) depending on the level of vacuum. At high vacuum the *Everhart-Thornley Detector* (ETD) is used and at low vacuum (evacuated to high vacuum and then water gas is released into the chamber) the *Large-Field Detector* (LFD) is used. Both are used for detecting *secondary electrons* (SE). The size of the grains is found from the SEM pictures produced by these detectors. The method applied is known as *average intercept length,* which is done along a random line on the micrograph. [6]

The microscope also has a detector for detecting the *back-scattered electrons* (BSE) (gives information about different phases). It is called a *Solid State Detector* (SSD).

The last detector that is used in the SEM is *Energy Dispersive Spectrometer* (EDS). It detects the x-ray signals emitted from the sample and then uses a software known as *EDAX* to figure out which elements are in the sample.

X-ray diffraction (XRD)

The characterisation of the pellets to find their crystal structure was done by the use of *Bruker D8 Apex 3-circle diffractometer, with monochromatic Cu-$K_{\alpha 1}$radiation and Bragg-Brentano geometry*, and the results were interpreted using the program *EVA Copyright © Bruker-AXS 1996-2007*.

[6] Brandon, D.G., Kaplan, W.D.. Microstructural Characterization of Materials. John Wiley & Sons Ltd; 2008.

The samples were mounted onto the stage of the machine and the spectra measurement for 2θ were $0° < 2\theta < 80°$.

Ellipsometry

The thickness of the thin films and their band gaps were measured using *alpha-SE®ellipsometer (J.A. Woolam Co. Inc., USA)* and the program used to interpret the results was *CompleteEASE*.

The thin films in this experiment were deposited on silicon wafers and fused silica glass. The samples that were used to determine the thickness of the film are the one that were deposited on silicon wafers. The samples on the silica glass were used to determine the absorption of the film and thereby approximating the value of the energy gap of the film.

X-ray Photoelectron Spectroscopy (XPS)

The machine used for this experiment was KRATOS AXIS ULTRA^{DLD} that uses monochromatic Al Kα radiation (hυ = 1486.6 eV). The spectra were acquired at a zero angle of emission, θ = 0°, (normal emission) with the lenses in hybrid mode (i.e. both magnetic and electrostatic lenses were used). In hybrid mode, the area of analysis was determines by the slot aperture (ca. 700 microns × 300 microns). The Al x-ray source was operated at 150 W. Survey spectra were acquired in the kinetic energy range of 0-1250 eV, and a pass energy of 160 eV with a step size of 1 eV. Data processing was performed using CasaXPS.[7]

The thin films were analysed by XPS to ascertain the elements present in the sample, the quantity of the different elements in the sample, and the chemical state of the elements in the sample. XPS is a surface analysis technique capable of probing ca. 1nm depth of the film.

[7] http://www.casaxps.com/

Photo-electrochemical measurements

Photo-electrochemical measurements were carried out on the thin films (TiO_2 and Nb-TiO_2) deposited on the FTO-glass. The samples were attached to a photo-electrochemical cell and used as working electrodes, while a platinum wire was used as the counter/auxiliary electrode. The reference electrode used for this experiment was a saturated calomel reference electrode (Hg_2Cl_2 is calomel). A copper strip is then glued onto the exposed part of the FTO-glass. This acts as a conducting pathway. The sample was pressed onto the bottom part of the cell with a with a sample holder that utilises a spring to accomplish this purpose. After the sample was in place, the electrolyte was poured in the cell and thereafter the counter and reference electrodes were placed in. Electrolytes with pH values of 2, 7 and 10 were used in the experiment. These electrolytes were buffer solutions.

pH value	Amount of chemical species per litre
2	793.651 mL, 0.2 M of KCl and 206.349 mL, 0.2M of HCl
7	632.111 mL, 0.1 KH_2PO_4 and 367.889 mL, 0.1 NaOH
10	823.723 mL, 0.05M $NaHCO_3$ and 176.277 mL, 0.1 M NaOH

The cell was placed under the solar simulator and the different electrodes were attached to the potentiostat. A test run was done to make sure that the sample was directly illuminated by the solar simulator.

After that the cell and window of the solar simulator were covered using aluminium foil paper to protect from harmful UV-radiation from the simulator. Thereafter the experiment commenced. The picture of the complete set-up is as shown in figure 2.

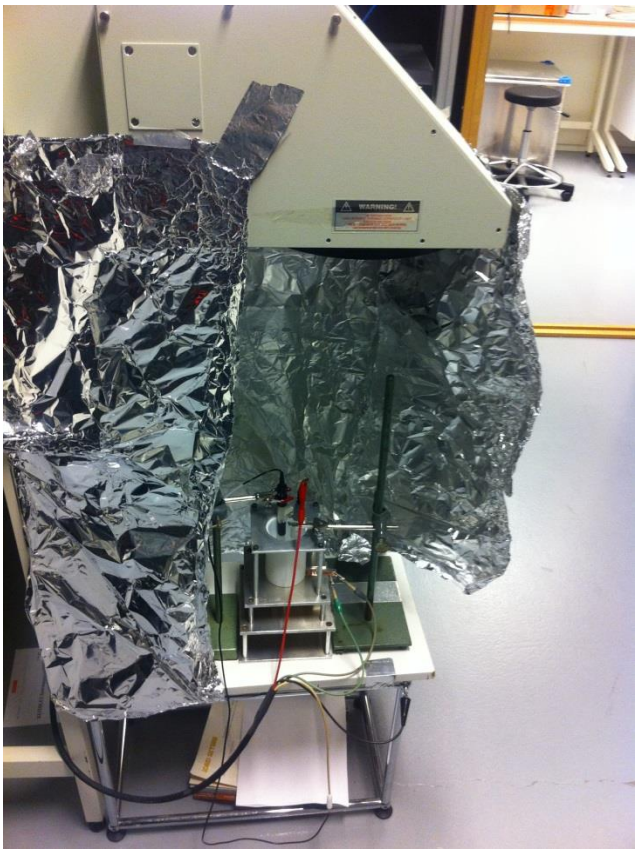

Figure 4: A picture of the solar simulator and photo-electrochemical cell set-up

The solar simulator had no filter. The light used is taken to be AM0 (meaning zero atmosphere).

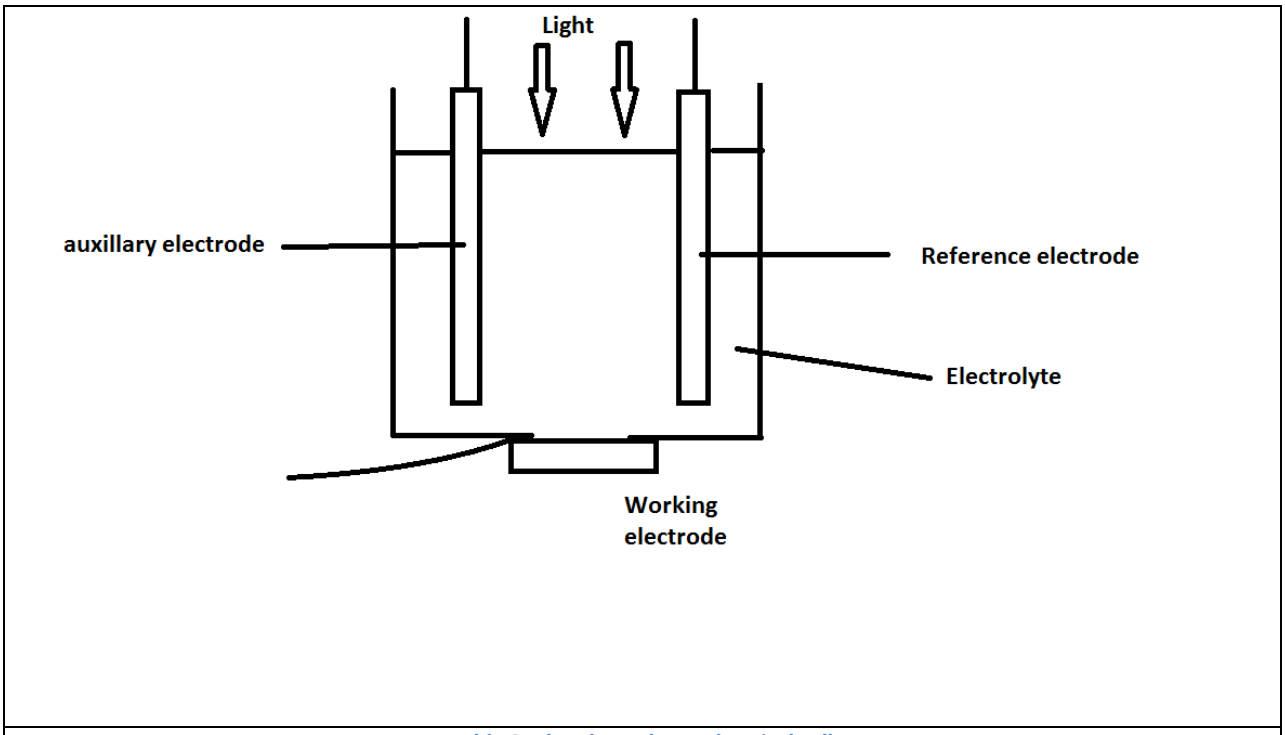

Table 3: The photoelectrochemical cell

5. RESULTS.

Structural Characterisation.

The three niobium doping levels in TiO_2 were, 1%, 3% and 30. In addition, undoped TiO_2 was used as a control to show that doping has an effect on the different studied properties. In the study of the structure of the compounds, the following analysis processes were employed: SEM, XRD, AFM and XPS.

Morphology.

The samples' morphologies were studied using SEM and AFM. The former method was used to check the grain size, phase composition and the morphology of both the pellets and the thin films. The EDS in the SEM was used to give an approximate value of the percentage elemental composition of the sample under analysis. The latter method (AFM) mentioned above was used to study the topology of the thin films.

The results from SEM of the samples (from undoped to 30% doped) are shown in figures 1-8. For each sample, micrographs from BCE, detected by SSD , are shown.

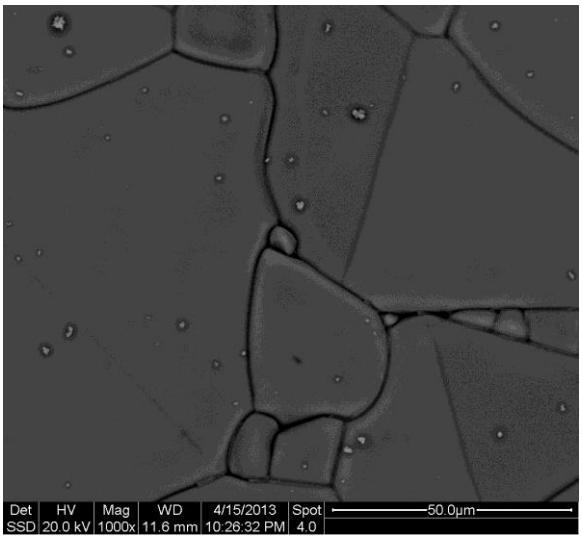

Figure 5: Unpolished undoped titania pellet. SSD

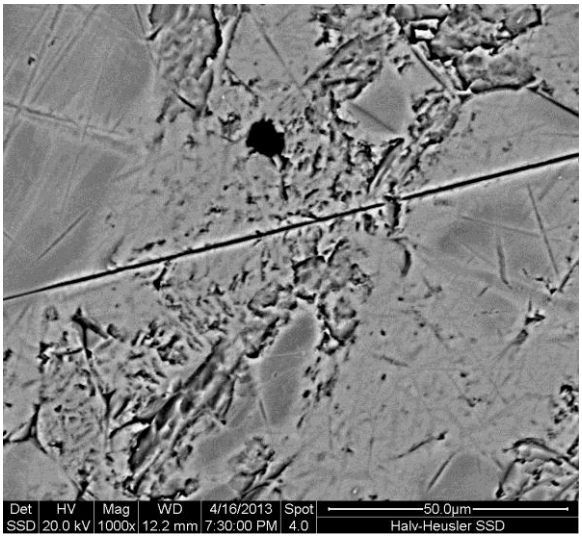

Figure 6: Polished undoped titania pellet. SSD

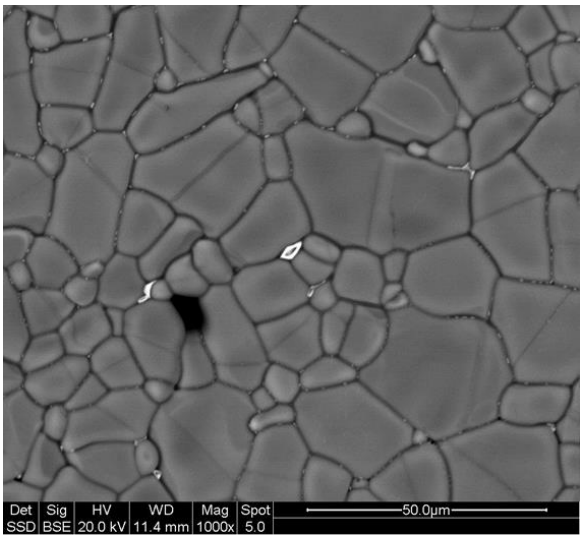

Figure 7: Micrographs of unpolished 1% doped titania pellet. SSD

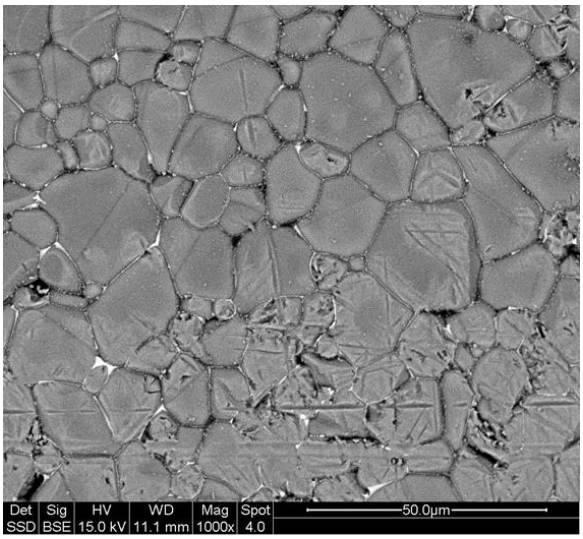

Figure 8: Micrographs of polished 1% doped titania pellet. SSD

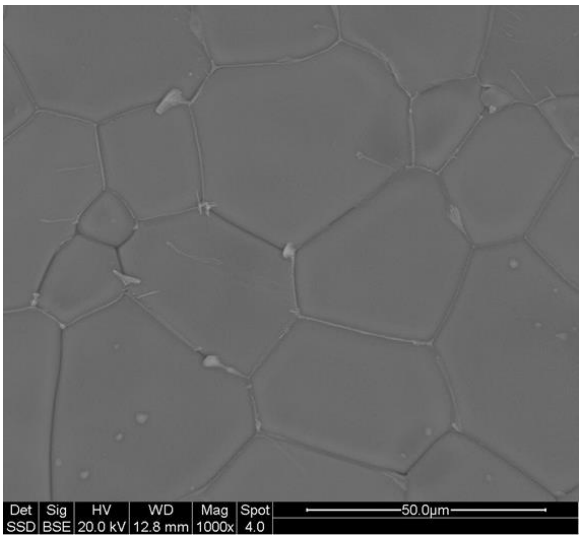

Figure 9: Micrographs of unpolished 3% doped titania pellet. SSD

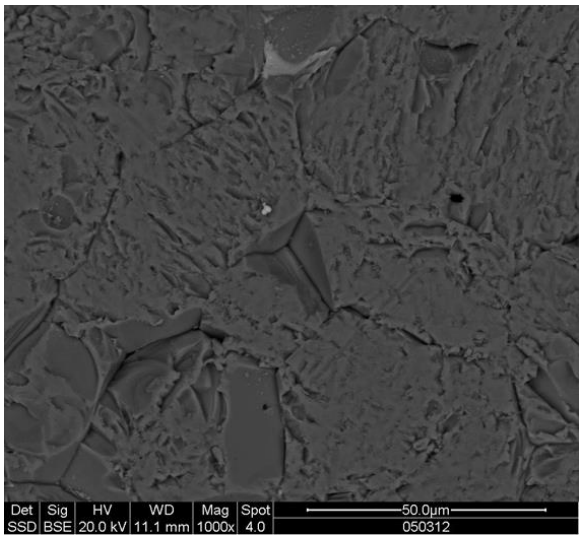

Figure 10: Micrographs of polished 3% doped titania pellet. SSD

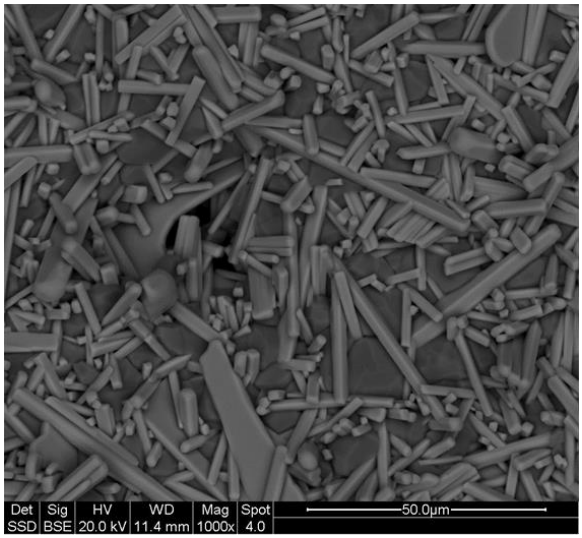

Figure 11: Micrographs of unpolished 30% doped titania pellet. SSD

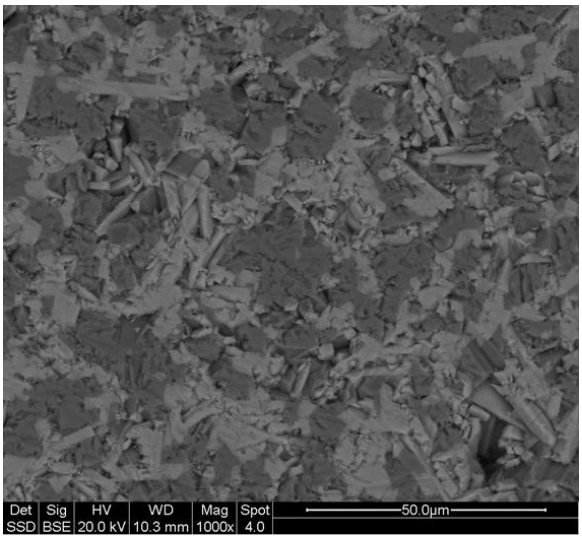

Figure 12: Micrographs of polished 30% doped titania pellet. SSD

All of the above micrographs were taken under low vacuum. The electron gun potential was 20 kV.

From the SSD micrographs of unpolished 1% and 3% samples (Figures 1 (a) and 3(a)), one can see secondary phases, predominantly in the grain boundaries, which are the lighter areas of the micrograph. The polished sample exhibit the same result. These are areas which are rich in niobium. This can be understood from the fact that back-scattered electrons are detected more from heavy elements, and thereby areas rich in niobium appear lighter than areas with less concentration of niobium. This was confirmed by EDS measurements of the lighter areas and it could be seen that the intensity from the niobium peaks in this region were higher than from the rest of the sample. (See Appendix)

The SSD micrograph of unpolished 30% sample shows some lighter (same hue different tones) crystalline material on top of a darker layer of grains. After polishing, it is seen that this phase continues beneath the surface of the sample and is not only a surface phenomenon. (Figure 6 (a)) One can still see some crystalline structure even after polishing. This phase is found out to be titanium niobate ($TiNb_2O_7$) as it will be shown using XRD analysis later.

Crystal Structure.

The crystal structure of the pellets was found using *X-ray diffraction* (XRD).

Below are diffractograms showing the different structures of the different samples.

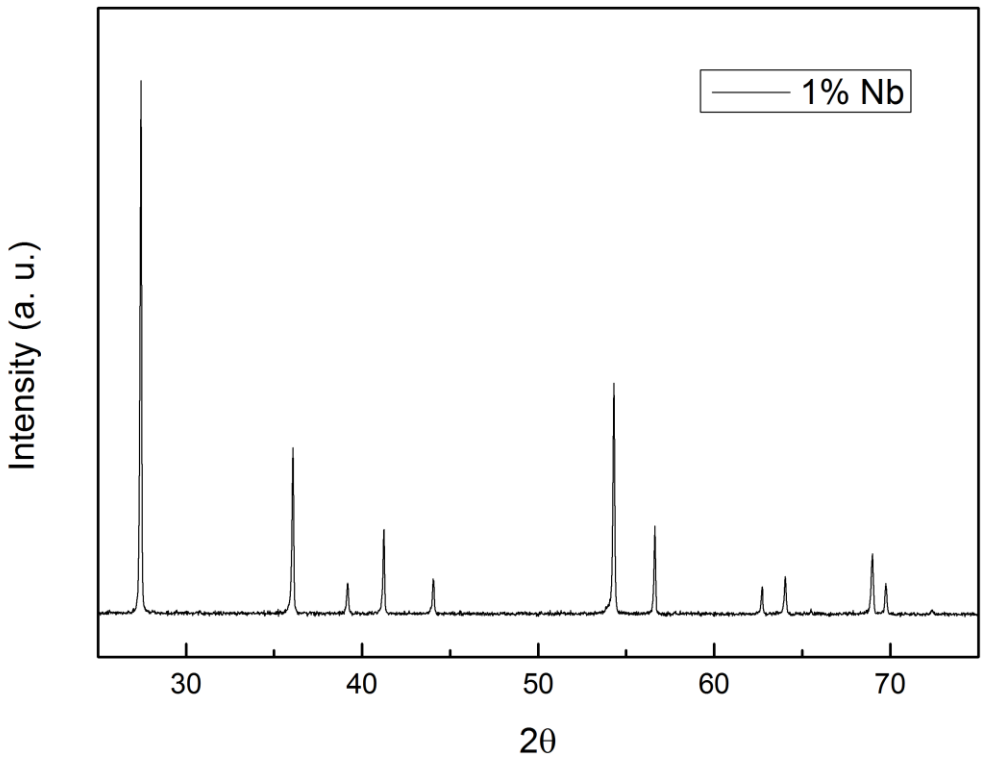

Figure 13: Diffractogram of 1% doped pellet

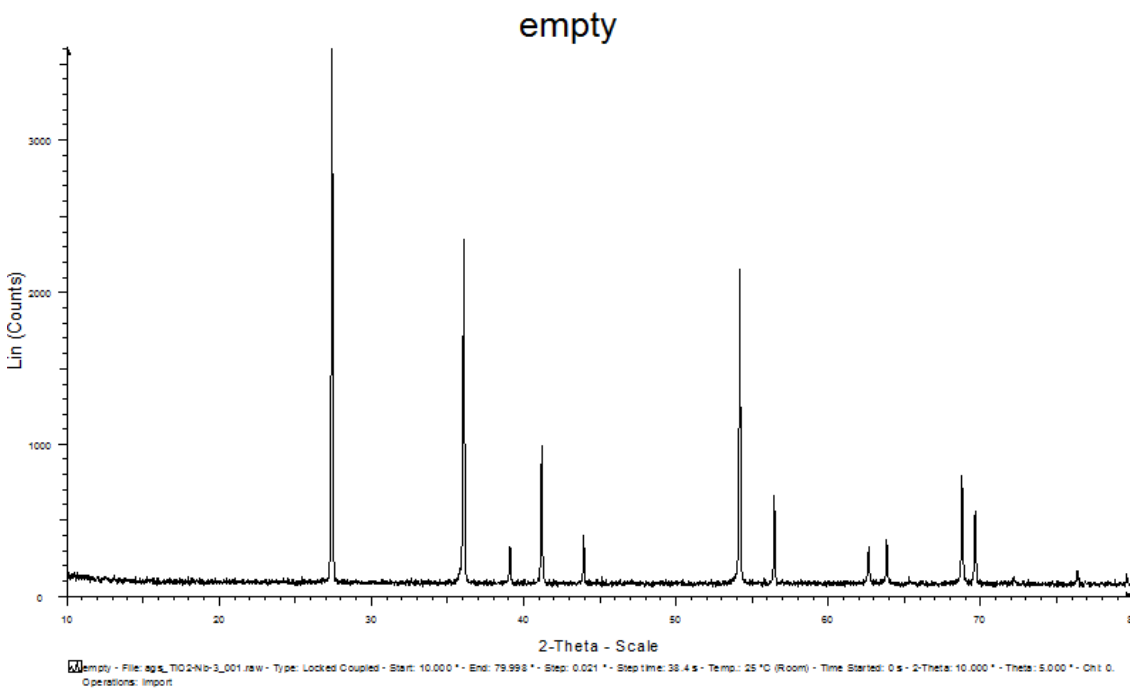

Figure 14: Diffractrogram of 3% doped pellet

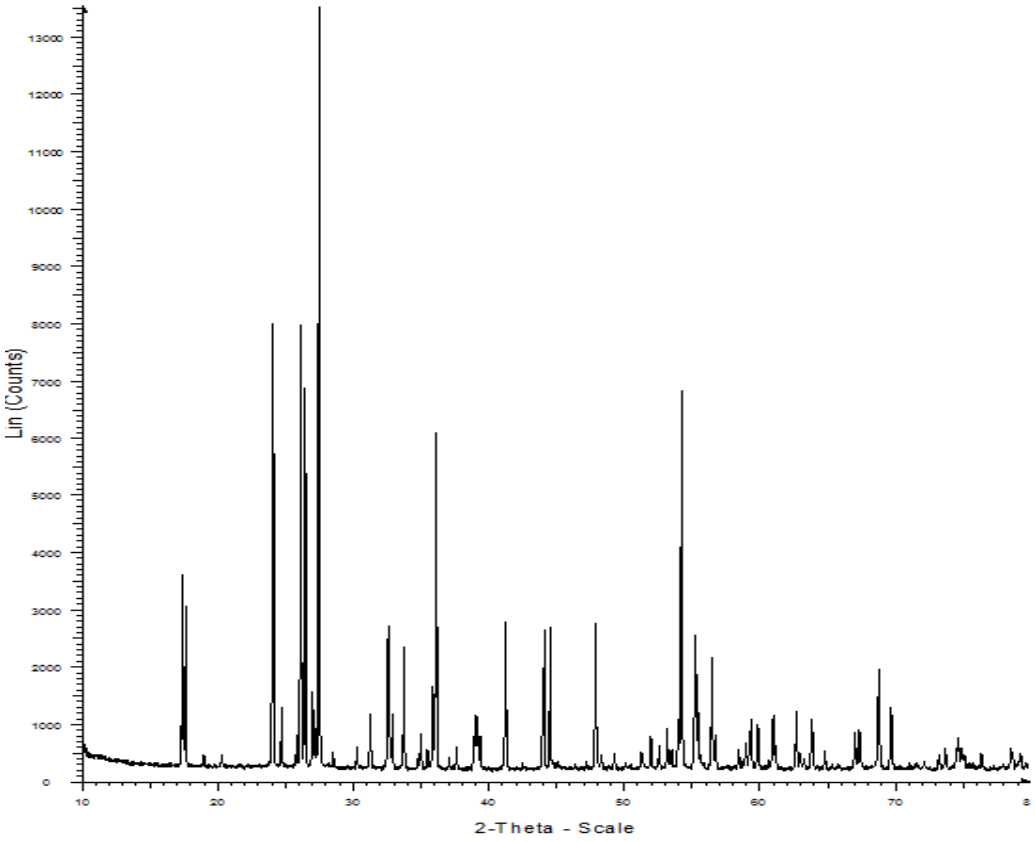

Figure 15: Diffraction of 30% doped pellet

Thin films

The thickness of the thin films as measured using ellipsometry, was found to be between 80nm and 100 nm.

Photo-activity of thin films

This section highlights the results that were acquired by studying the samples both with and without irradiation. The samples were studied to gain insight on the effects of pH, doping, and light on photocurrent, and flat-band potential. The area of the sample irradiated is 1 cm^2.

Effect of pH on IV characteristic graph.

The effect of pH on the IV characteristic graph is the first experiment. The three chosen pH conditions were 2, 7 and 10.

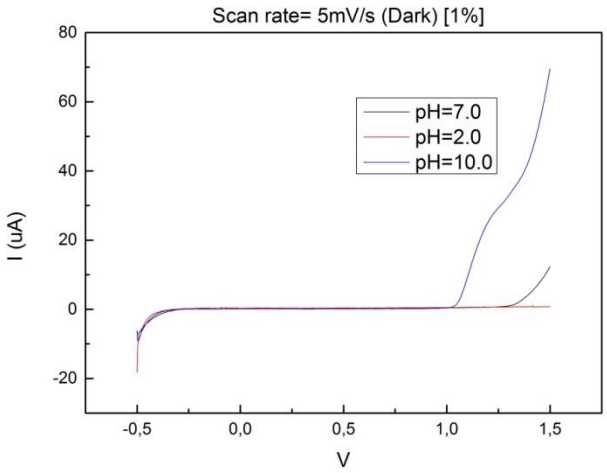

Figure 16: Effect of pH on IV characteristic graph (1%)

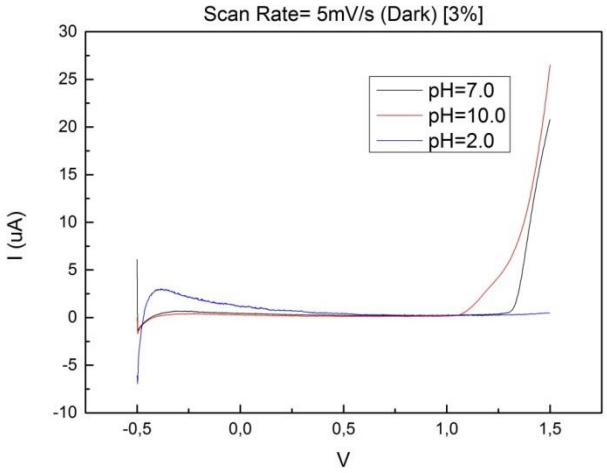

Figure 17: Effect of pH on IV characteristic graph (3%)

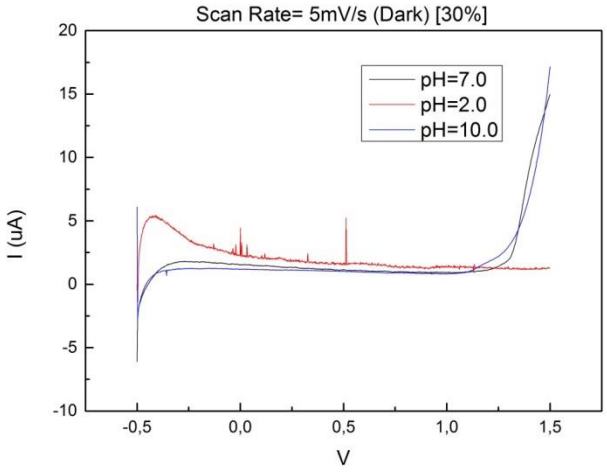

Figure 18: Effect of pH on IV characteristic graph (30%)

From the above graphs it can be seen that the best pH for electrolysis is 10 and will thus be used for further studies. This is because the electrolytic potential is reduced as compared to the other two pH values. This can be seen for all the samples.

Effect of light on photocurrent.

The effects of light on the photocurrent are shown for pH = 10. Reasons being that this is the pH chosen to do other experiments hereafter. The effect of light shall be shown for the different doping percentages, namely 1%, 3% and 30%.

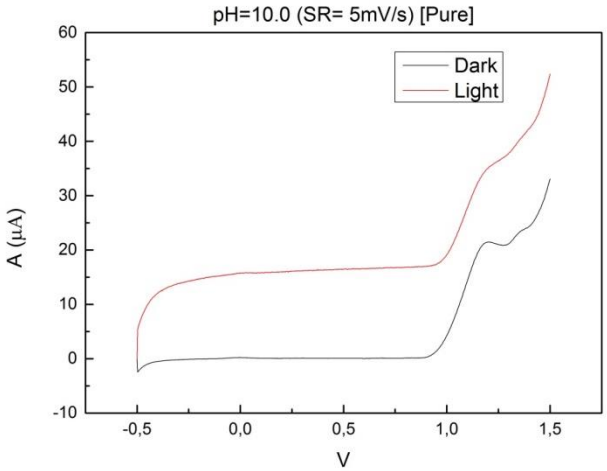

Figure 19: Light and dark IV characterstic graph (undoped)

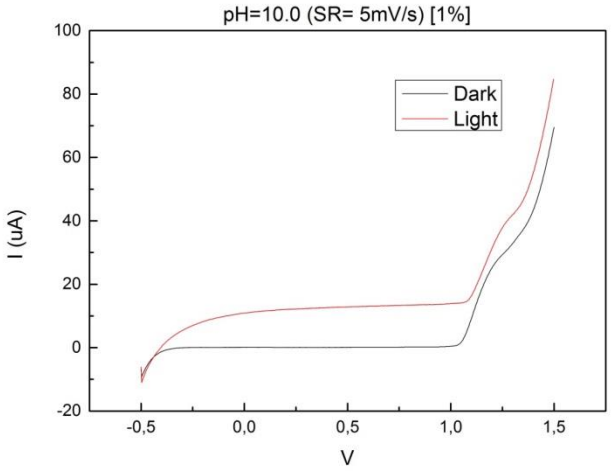

Figure 20: Light and dark IV characteristic graph (1%)

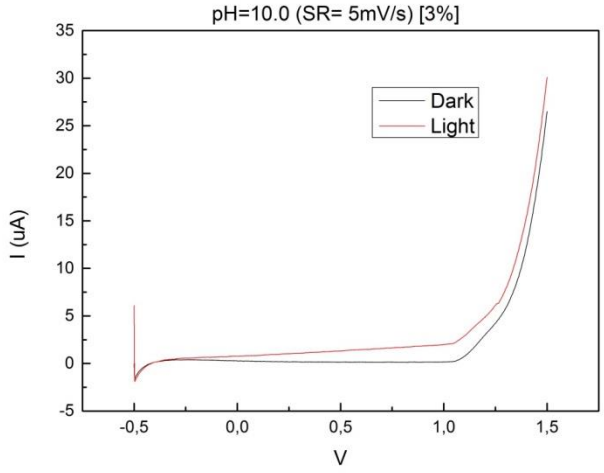

Figure 21: Light and dark IV characteristic graph (3%)

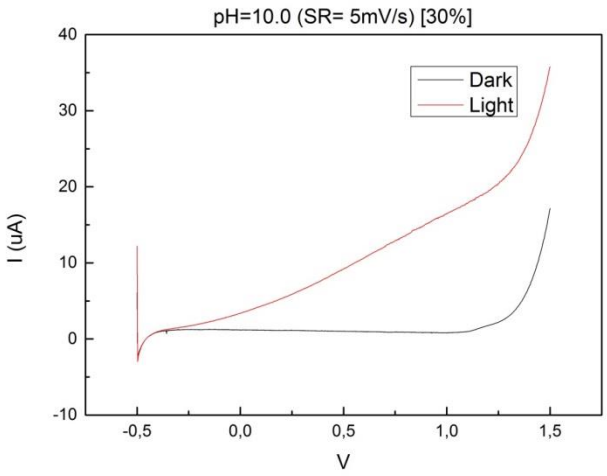

Figure 22: Light and dark IV characteristic graph (30%)

From the diagrams 10,11 and 12 it can be seen that the photocurrent increase when light is shone on the sample. It can also be seen that the photocurrent reduces when doping is increased from 1% to 3% (Diagram 10 and 11 respectively). For the 30% doped sample the trend is not easily noticeable (Diagram 12).

Chronoamperometry.

In this technique the potential of the working electrode (undoped titania and niobium-doped titania) is changed from the initial potential to a chosen potential step. The potential is maintained at the potential step for the remainder of the experiment. While the potential step is held constant, the current of the working electrode is measured with light off and on against time. The two potential values chosen are 0V and 0.5V.

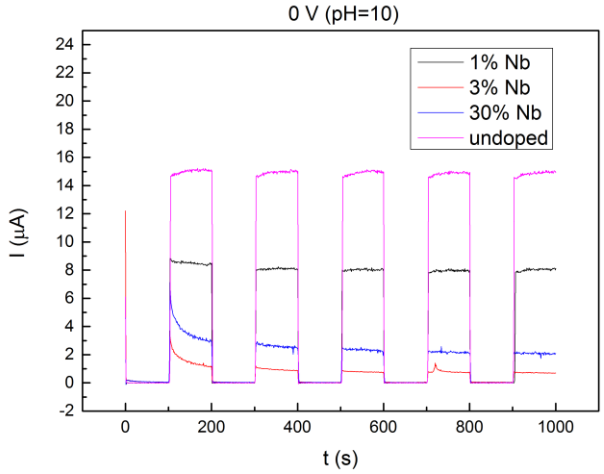

Figure 23: Chronoamperometry graph at 0V

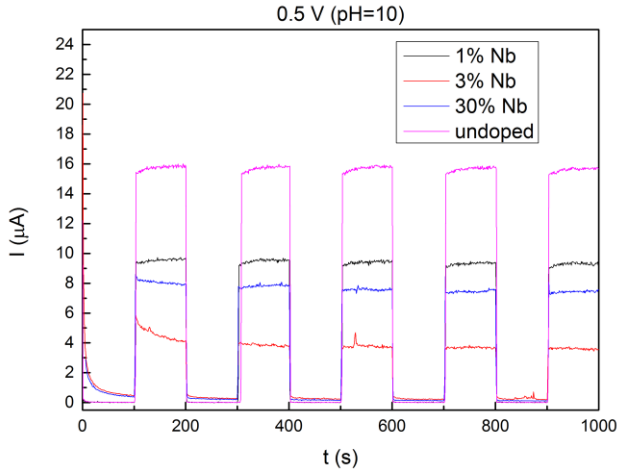

Figure 24: Chronoamperometry graph at 0.5V

From the diagrams 13 and 14, it can be seen that the increase in potential step leads to increase of current measured on the working electrode. The current produced decreases as the doping level increases, except for 30% doping.

Mott Schottky analysis.

This technique was used so as to verify the flat-band potentials of the different samples (1%, 3% and 30%). Inverse capacitance is measured against potential. The flat-band potential is the x-intercept of the graph.

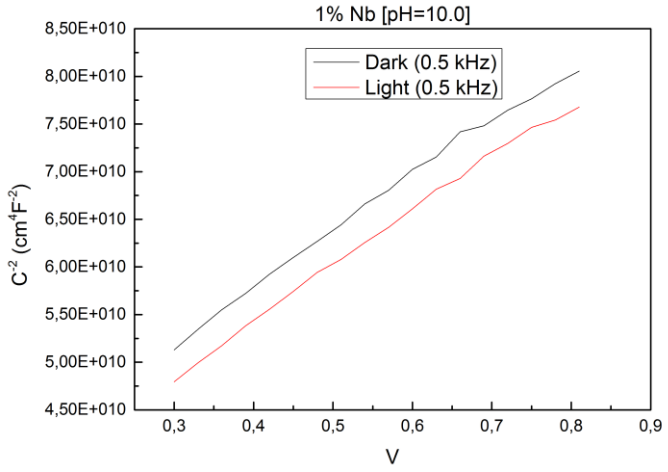

Figure 25: Mott Schottky graph of 1%

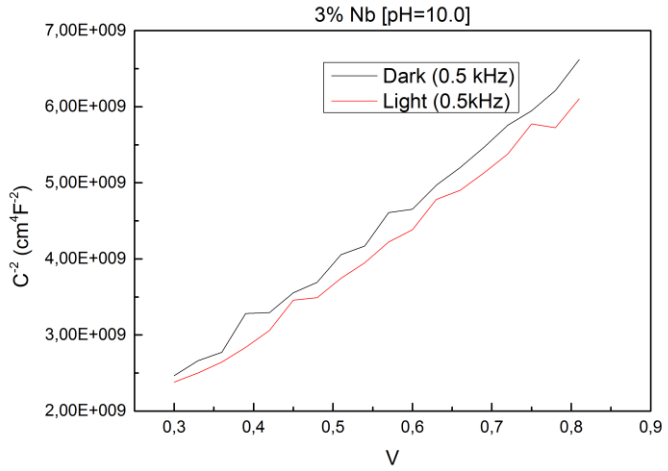

Figure 26: Mott Schottky graph of 3%

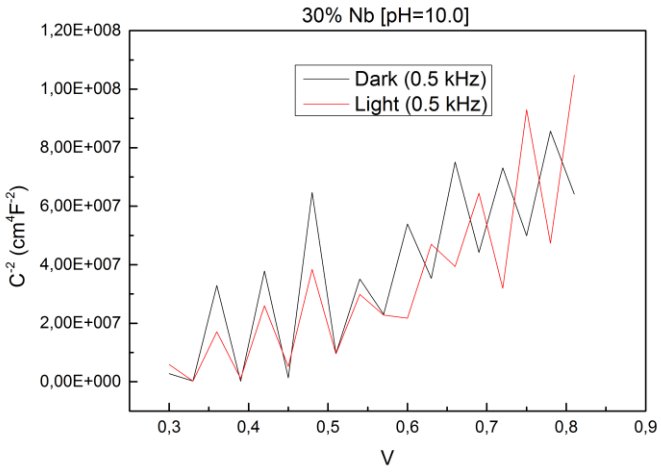

Figure 27: Mott Schottky graph of 30%

The experiment was carried out using frequencies of 0.5 kHz and 1kHz. It was also done with light off and on.

X-ray photoelectron spectroscopy (XPS).

This technique was used to verify the amount of niobium in the different thin film samples (elemental composition) and to find out the chemical states of the constituent elements.

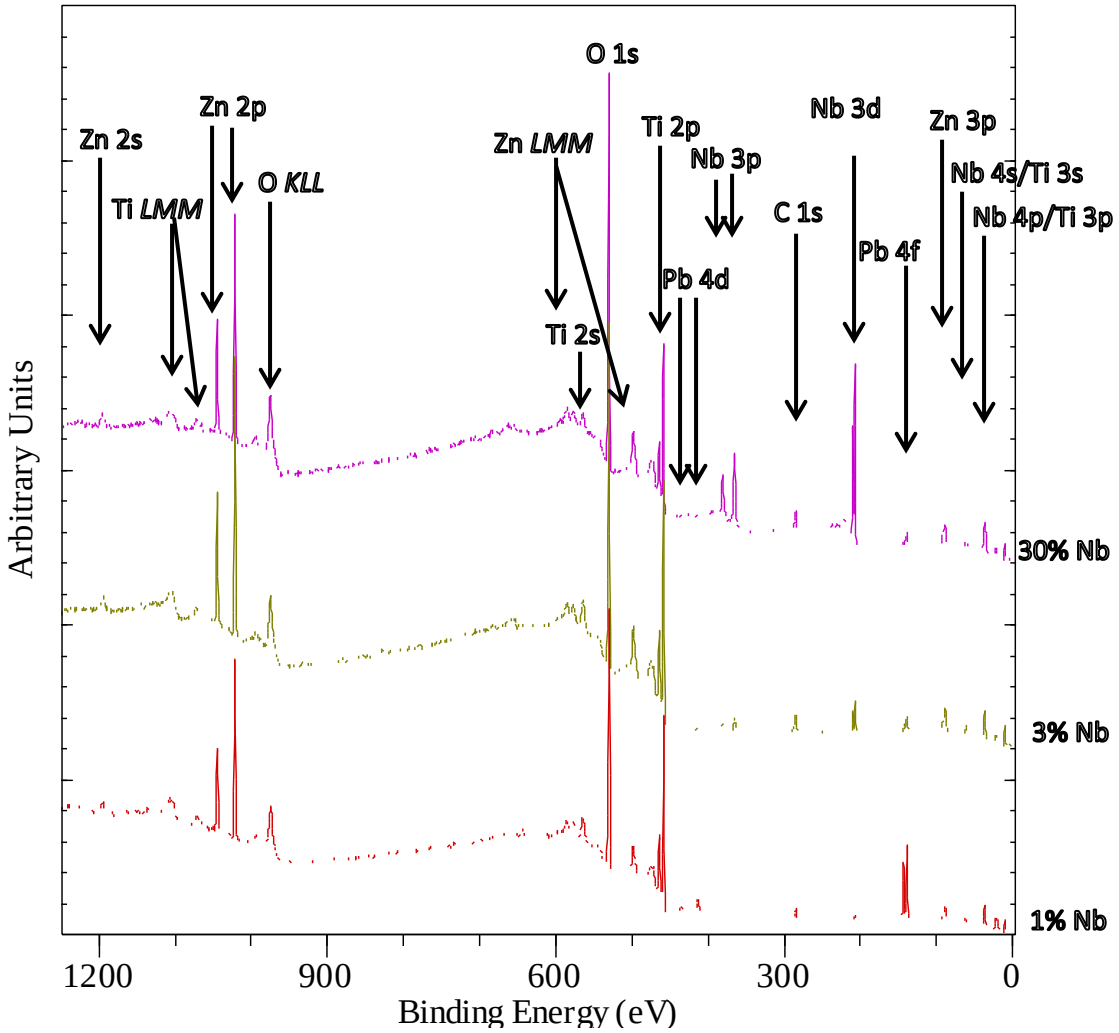

Figure 23: Survey scans of the samples analysed showing the main elements present on the surface.

The above diagram shows the survey scan of three samples (1%, 3% and 30%). These are all the peaks detected and the corresponding energy shells from different elements. It show the expected elements (Ti, Nb and O) and some impurities (Pb).

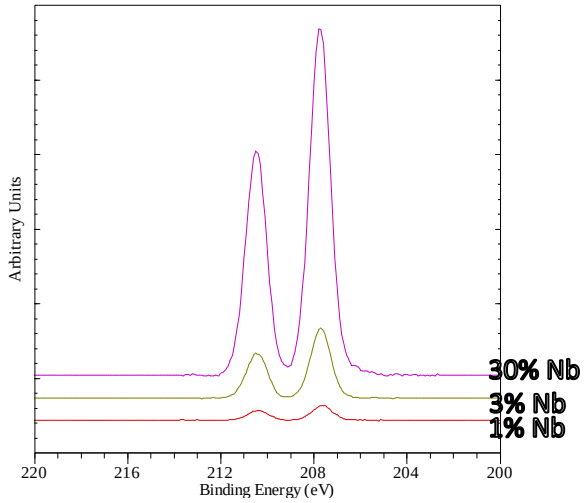

Figure 24: High resolution Nb 3d spectra after subtraction of a Shirley type of background, showing different intensities owing to different Nb contents.

The above diagram shows the intensities from Nb 3d and it can be seen that the intensity increases as the doping level increases.

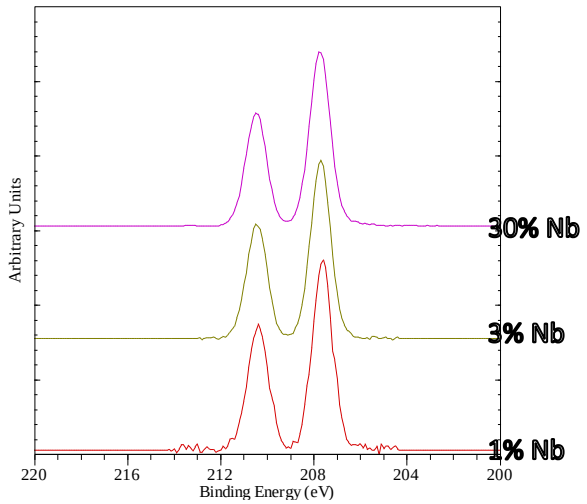

Figure 25: Same as above (19) but now the spectra are normalized for the same intensity.

The binding energy of Nb 3d in all three samples is not shifted and the peak widths are the same, showing that Nb exist in the same chemical state in all samples. This corresponds to the +5 oxidation state.

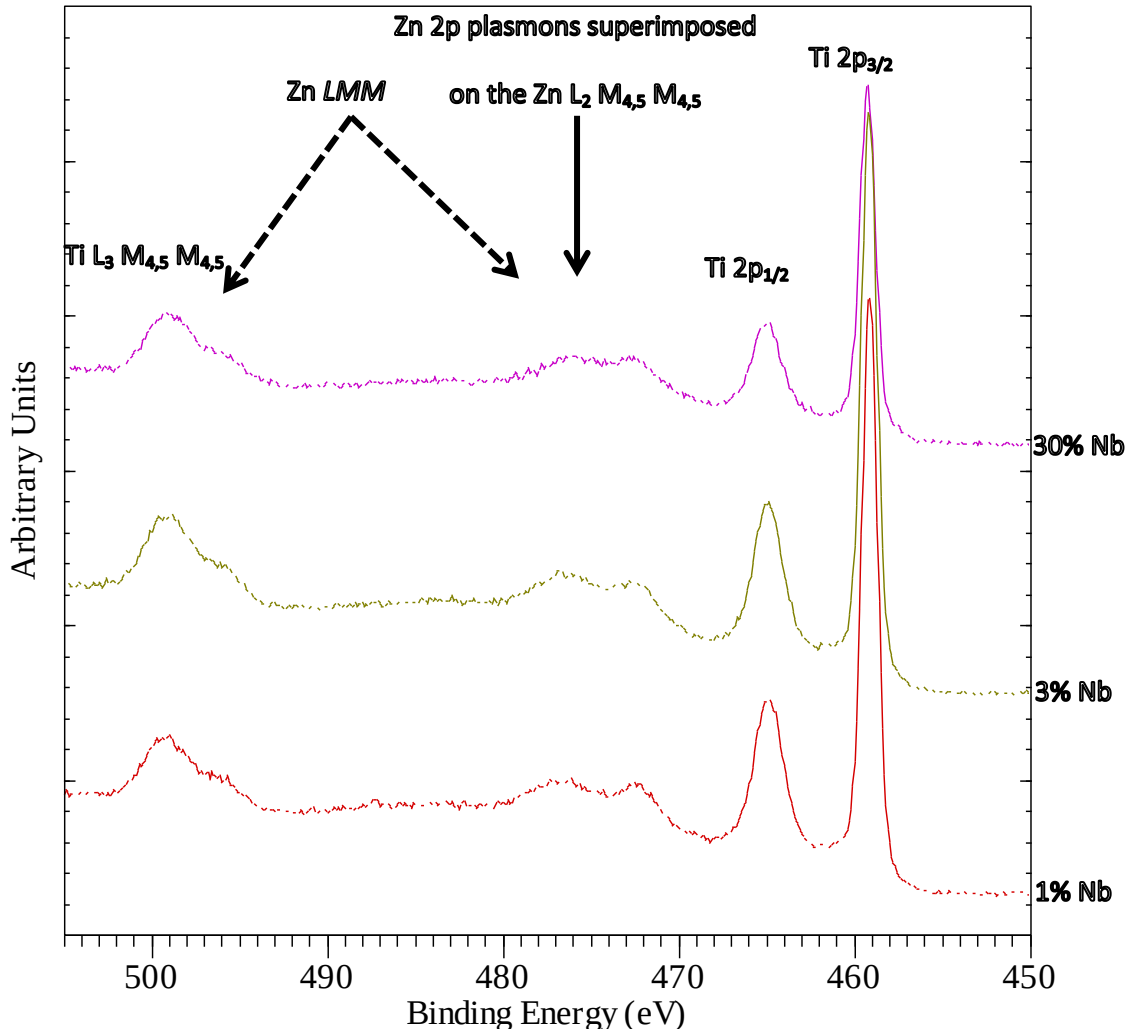

Figure 26: High resolution Ti 2p peaks together with Ti LMM Auger peaks and Ti 2p plasmons.

Like for the Nb peaks, the Ti 2p peaks are not shifted and the peak width is similar. The peak positions correspond to +4 oxidation state of Ti.

6. DISCUSSION.

Structural analysis.

The pellets of 1%, 3% and 30% Nb-doped TiO_2 were analysed using SEM and different surface structures and phases were observed. For the 1% and 3% doped pellets it could be seen that there was segregation of niobium rich compound into the grain boundaries. This conclusion was reached to, by considering the difference in tone of these areas as compared to the rest of the bulk material from the SSD, and by carrying out EDS analysis (Appendix). As mentioned in **the results section**, the lighter the area, the heavier the element, in this case niobium. (**Results**: Fig. 3 &5) From the EDS spectra, one could also observe that there are more signals from the presumed niobium rich areas than from the rest of the bulk. For better results transmission electron microscopy could have employed to find out its structure. The pictures of 1% and 3% Nb-doped TiO_2, figures 3 and 5 respectively, can be compared to figure 1 of undoped TiO_2, which contains no lighter areas in the grain boundaries. The lighter particulates in figure 1 could not be identified as the EDS analysis from them was the same with the rest of the bulk material. These may be impurities on the surface as they are not observed in the micrograph of the polished pellet (Figure 2). Niobium segregation has been studied by Sheppard et al.(Sheppard 2013) (Sheppard, Dittrich et al. 2012). In his paper he concludes that the partial pressure of oxygen ($O_{2(g)}$) is directly proportional to the amount of niobium segregated on the surface and interfaces, i.e. the higher the partial pressure the more the segregation. Sintering was carried out under atmospheric pressure. This means that the partial pressure of oxygen is 21kPa and this is found using the following formula:

$$p_i = p_{total} \times x_i$$

where p_i is partial pressure of species i, p_{total} is the total pressure of the mixture and x_i is the mole fraction of i.

The pressure at which the effects of high and low oxygen activity are differentiated is 1 Pa. Niobium dissolution into titania proceeds in two different ways in the two different conditions.

$$2Nb_2O_5 = 4\,Nb^{\bullet}{}_{Ti} + 10{O_O}^{x} + {v_{Ti}}''''$$

High oxygen activity

$$Nb_2O_5 = 2Nb^{\bullet}{}_{Ti} + 2e' + 4O^{x}{}_{O} + \frac{1}{2}O_{2(g)}$$

Low oxygen activity

The conditions under which the pellets in this experiment were sintered can thereby be defined as having a high oxygen activity. This leads to the formation of donor niobium atom ($Nb^{\bullet}_{Ti}$) and titanium vacancies as compensating charge defects ($v^{////}_{Ti}$). Despite the segregation, the structure of the pellet as observed from x-ray diffraction (XRD) is the rutile structure, which is the structure of undoped titania.

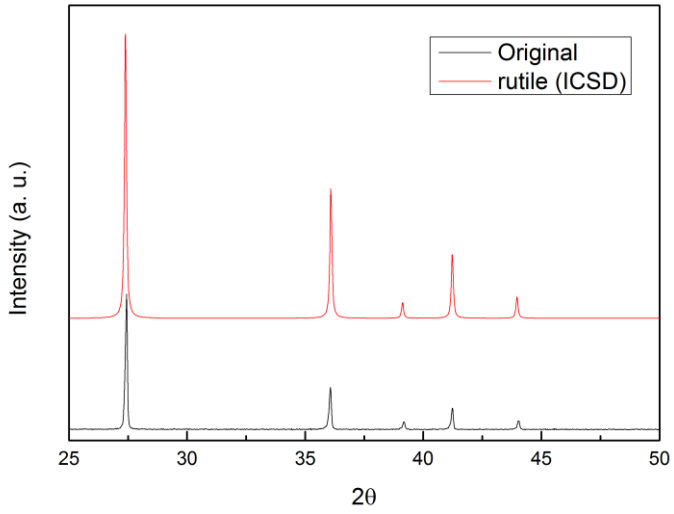

Figure 28: Comparison between XRD spectrum of 1% pellet (Original) to XRD spectrum of rutile from ICSD database (Similar to 3%)

The microrod structures in the 30% niobium-doped titania are understood to be titanium niobate ($TiNb_2O_7$), while the rest is Nb-doped TiO_2. This is shown by the results from XRD. It can be seen that there is both rutile and $TiNb_2O_7$ structure.

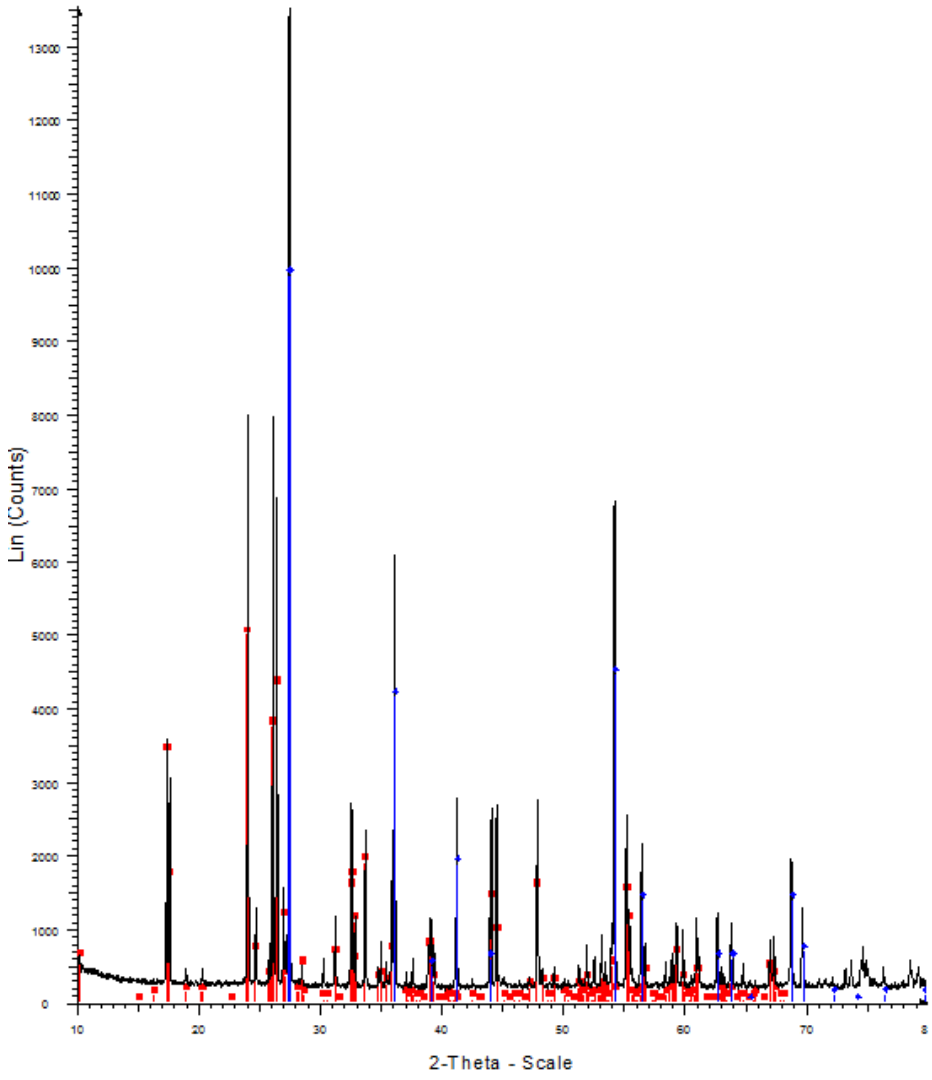

Figure 29: Comparison between XRD spectrum of 30% pellet (Original) to XRD spectrum of rutile (blue) and titanium niobate (red) from ICSD database

Thin films.

The thin films were found to have a thickness of 80-100 nm. They were deposited on a conducting substrate of FTO-glass at 450. At this temperature the films will be amorphous. This was shown by work done by Ok et.al (Ok, Park et al. 2012). They showed that the Nb-doped titania films remain amorphous up to at least temperatures of 450°C. XRD was not performed on my films to check this, but the deposition temperature was within their range.

The calculated band gap from absorption measurements by use of ellipsometry was found to be around 3.0 eV.

Photo-activity of the thin films.

The first investigation on the thin films was to find the optimal or best pH. This was done in electrolyte of pH 2,7 and 10. The pH value with the lowest oxidation potential was considered the best. The effect of pH on oxidation potential can be explained using the Nernst equation.

$$E = E_0 + \frac{RT}{nF} \ln Q$$

E is, in this case, the oxidation potential, E_0 is the standard electrode potential, R is ideal gas constant, n is number of electron moles, F is Faraday's constant and Q is the reaction coefficient. In terms of pH, the equation is written as such,

$$E = E_0 - 2.3 \frac{RT}{nF} pH$$

The decrease in oxidation potential with increase in pH is elucidated by the equation. Therefore pH 10 was chosen to carry out the remaining photo-catalytic experiments.

From figures 14-17 in the results section it can be seen that upon illumination charge carries are created and thus leading to the increase of current from zero to different values in the different films with different doping quantities. This is due to the separation of the two created charge carriers, i.e. electron and hole, near the surface of the film. This separation is brought about by the potential that is created at the interface region between the semiconductor and the electrolyte due to band bending. The hole migrates towards the surface while the electron migrates into the semiconductor. (Bott 1998)

$$TiO_2 + h\upsilon \rightarrow e^- + h^+$$

At the TiO_2 electrode

$$2H_2O + 4h^+ \rightarrow O_2 + 4H^+$$

At the platinum (Pt) electrode

$$4H^+ + 4e^- \rightarrow H_2$$

The current produced by light is described as follows,

$$I_{ph} = eI_0[1 - (1 + \alpha L_p) \cdot e^{-\alpha w}]$$

Where α is the light absorption coefficient, L_p is the hole diffusion length, w is the space charge region length.

Where

$$L_p = (D_p \tau_p)^{1/2} = (kT \cdot \mu_p \tau_p)^{1/2}$$

Where μ_p is the hole mobility, τ_p is the lifetime of the hole and D_p is the diffusion coefficient of the hole.

The light absorption coefficient is dependent on the energy of the incident photon and the band gap.

$$\alpha = A\sqrt{h\upsilon - E_{BG}}$$

Photons with high energy have a better absorption coefficient and so do materials with small band gaps. This will be useful when looking at the chronoamperometry values of the different samples.

One can also observe that after the onset of electrolysis (around 1V) in the undoped and 1% doped films, the is a change in the slope of the graph. This could be the oxidation of another anion in the electrolyte. In this case, that would be the hydrogen carbonate anion (HCO_3^-). I could not find the reduction potential of either HCO_3^- or carbonate (CO_3^-) and thereby could not verify my assumptions. But seeing that the aforementioned anions are the only choices left, it may be wise to assume that they are being oxidised.

On the negative potential side of the graph, the deep or change in slope can be attributed to charging of the surface. It can also be hydrogen evolution, but TiO_2 is not as good a material as Pt at evolving hydrogen.

The almost vertical lines in the beginning of some of the graphs are just set starting values during the measurement. The region where both light and dark intersect at 0 A is defined as the flat-band potential. This is the potential that counteracts the band bending potential. Therefore, even if light is shone on the material, no current is registered due to the lack of potential to separate the charge carriers at the interface and they thereby recombine.

The results from the chronoamperometry show that the current produced by undoped TiO_2 is more than for the doped samples. This is counter to what one would expect. Doping increases the number of free charge carriers. One would expect a higher current in the doped samples as compared to the undoped sample. One explanation for this conundrum would be that in the pure TiO_2 there would be small amount of impurities which would act as dopants thus producing extra charge carriers. The list of impurities in the TiO_2 I used was not listed. But even if that was the case, then there would have been a likelihood of this being reported in other studies. The other explanation could be the Burstein-Moss shift. In this case, if one increases the amount of doping, then the newly created energy states are formed in the conduction band and thereby increase the band gap and less charge carriers are created. Whether this is the case with the undoped and doped sample is unclear and more research needs to be carried out to verify. The comparison of the photocurrent between the doped samples can be explained by Burstein-Moss shift.

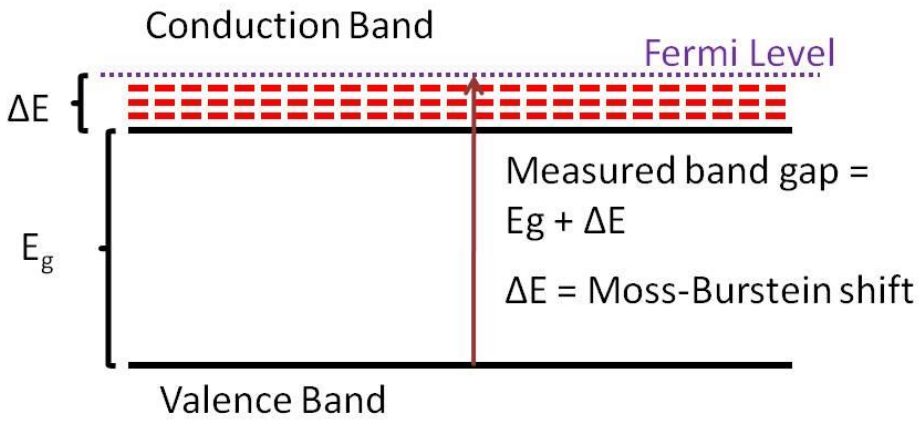

Figure 30: A figure depicitng the Burstein-Moss shift[8]

The minimum photon energy for excitation is therefore:

$$h\upsilon_{min} = E_g + \frac{\hbar^2 {k_F}^2}{2}\left(\frac{1}{m_c} + \frac{1}{m_v}\right) = E_g + E_F\left(1 + \frac{m_c}{m_v}\right)$$

As the Fermi level increases, so does the energy of the photon required to excite and electron from the valence band edge to the conduction band.

From the chronoamperometry graph we see that the highest current of the doped samples is that of 1% doping. If we assume that the current is 1μA then one could try to find out how long it would take to form a bubble of hydrogen with the diameter 5mm.

Assume the bubble is a sphere.

$$V = \frac{4}{3}\pi r^3 = \frac{\pi}{3} \times 10^{-11} m^3$$

It is assumed that this is taking place at ambient temperature and pressure.

1 mol = 24 dm^3

$$\frac{\pi}{3} \times 10^{-11} m^3 = \frac{\pi}{7.2} \times 10^{-9}\ moles\ of\ H_2$$

[8] http://en.wikipedia.org/wiki/Burstein%E2%80%93Moss_effect (12/08/2013)

Moles of electrons = 2× moles of H_2 $= \frac{\pi}{3.6} \times 10^{-9}\ moles$

Charge needed

$$C = \frac{F}{N_A \times mol\ of\ e} \approx 1.835 \times 10^{-10} C$$

Time needed to produce the bubble is

$$t = \frac{Charge}{Current} = 1.835 \times 10^{-5} s$$

It would basically take 2days 10 hours to get a mole of hydrogen. And we have disregarded the inefficiencies of charge transfer, which would make it longer. This calculations are done for $1cm^2$ area of the sample. As shown by Khan et. al increase in surface area like using nanorods will increase the rate of production. (Alam Khan, Shaheer Akhtar et al. 2008)

It can also be observed that as the applied voltage increases, so does the current. This is because there is less charge recombination due to the increase of the space charge layer potential.

$$V_E = \phi_{SC} + V_{FB}$$

Where V_E is the external or applied voltage, ϕ_{SC} is the potential of the space charge layer and V_{FB} is the flat-band potential.

From Mott-Schottky analysis the flat-band potential of the films can be calculated. The calculated flat-band potentials were as follows:

Sample	**Flat-band potential (V)**
1%	-0.603
3%	0.025
30%	0.269

X-ray photoelectron spectroscopy.

From the results from XPS one can see peaks from both Ti and Nb with some impurities of Pb and Zn. Apart from the Pb and Zn, the other results are expected. On a closer look at the Nb 3d peaks from the three different samples have different intensities. The highest being from 30% and the lowest from 1%. This shows that the amount of Nb increases as expected. The peak position (binding energy) of the Nb 3d peaks verify that the chemical state of Nb is Nb^{5+}. This is the expected chemical state of Nb when it is substitutes Ti in a rutile structure. This proves that the samples are n-type semiconductors.

The Ti 2p peaks also show that the chemical state of Ti is Ti^{4+}, which is the expected chemical state of Ti in rutile. This further strengthens the argument of the material being a n-type semiconductor.

Further study.

To get more homogeneous pellets without segregations a study on the effects of the surroundings on the diffusion of Nb in TiO_2 will have to be studied. In addition, lower doping levels might be necessary to explore as it has been shown that increase in doping level leads to the decrease in photocurrent.

Increasing the surface area of the thin films by creating nano-sturctures such as nanorods could increase its efficiency as the diffusion length of the charge carriers are reduced and the surface area interacting with light is increased.

Alam Khan, M., et al. (2008). "Enhanced photoresponse under visible light in Pt ionized TiO2 nanotube for the photocatalytic splitting of water." Catalysis Communications **10**(1): 1-5.

Bott, A. W. (1998). "Electrochemistry of semiconductors." Current Separations **17**: 87-92.

Ok, K.-C., et al. (2012). "Semiconducting behavior of niobium-doped titanium oxide in the amorphous state." Applied Physics Letters **100**(14): 142103-142103.

Sheppard, L. (2013). "Niobium Surface Segregation in Polycrystalline Niobium-Doped Titanium Dioxide." The Journal of Physical Chemistry C **117**(7): 3407-3413.

Sheppard, L. R., et al. (2012). "The Impact of Niobium Surface Segregation on Charge Separation in Niobium-Doped Titanium Dioxide." The Journal of Physical Chemistry C **116**(39): 20923-20929.

7. CONCLUSION.

Thus far it can be seen that the samples are n-type semiconductors, and that the higher the doping level, the lower the photocurrent as explained using the Burstein-Moss shift. It is still unexplainable why the undoped sample has a higher current than the doped samples, but two theories have been put forward and more research needs to be done on it. The photocurrent produced under what can be considered close to sunlight, is still not enough to have any feasible commercial production of hydrogen.

In terms of synthesising the material for use as a target for thin film production, we see that the Nb does not completely dissolve into the material and therefore it might be prudent to carry out experiment by controlling the environment of the synthesis in order to find out the favourable conditions for making a homogeneous solid solution. The amount of doping can also be reduced to see whether the photocurrent will increase, because as per the results found here, it does not look like a viable replacement for other forms of energy sources.

Thin films give us a certain amount of current, albeit not enough. It has been shown that the making of thin films with different nanostructures, increases the surface area, which will give more area to allow photo-excitation and also reduce the required diffusion length of the created photo-generated charge carriers. This will lead to increase efficiency and increase in generated current that might end up being enough for commercial generation of hydrogen.

The study has shown that more needs to be done in order to increase the efficiency of hydrogen production through the photocatalysis of water. This will thereby lead it to being a competitor in the energy market.

8. REFERENCE LIST.

Depero, L. E., et al. (1998). "Niobium-titanium oxide powders obtained by laser-induced synthesis: Microstructure and structure evolution from diffraction data." Journal of Materials Research **13**(06): 1644-1649.

Hanaor, D. H. and C. Sorrell (2011). "Review of the anatase to rutile phase transformation." Journal of Materials Science **46**(4): 855-874.

Ok, K.-C., et al. (2012). "Semiconducting behavior of niobium-doped titanium oxide in the amorphous state." Applied Physics Letters **100**(14): 142103-142103.

Sheppard, L. (2013). "Niobium Surface Segregation in Polycrystalline Niobium-Doped Titanium Dioxide." The Journal of Physical Chemistry C **117**(7): 3407-3413.

Sheppard, L. R., et al. (2012). "The Impact of Niobium Surface Segregation on Charge Separation in Niobium-Doped Titanium Dioxide." The Journal of Physical Chemistry C **116**(39): 20923-20929.

Yang, Z., et al. (2009). "Nanostructures and lithium electrochemical reactivity of lithium titanites and titanium oxides: A review." Journal of Power Sources **192**(2): 588-598.

Alam Khan, M., et al. (2008). "Enhanced photoresponse under visible light in Pt ionized TiO2 nanotube for the photocatalytic splitting of water." Catalysis Communications **10**(1): 1-5.

Bott, A. W. (1998). "Electrochemistry of semiconductors." Current Separations **17**: 87-92.

Ok, K.-C., et al. (2012). "Semiconducting behavior of niobium-doped titanium oxide in the amorphous state." Applied Physics Letters **100**(14): 142103-142103.

Babich, T. G., Zagorodnyuk, A. V., Teterin, G. A., Khodos, M. Y., Zhirnova, A. P. Russ J Inorg Chem (Engl Transl). 1988;33(4):3.

Grimes, C. A., Ranjan, S., Varghese, O. K. *Light, Water, Hydrogen: The Solar Generation of Hydrogen by Water Photoelectrolysis.* Springer Science+Business Media, LLC; 2008.

Nygård, I.H.. Electrical characterisation of grain boundaries in donor doped TiO_2. Master of Science, University of Oslo, 2012.

Brandon, D.G., Kaplan, W.D.. Microstructural Characterization of Materials. John Wiley & Sons Ltd; 2008.

CASAXPS http://www.casaxps.com/

Hashimoto, K., et al. (2005). "TiO~ 2 Photocatalysis: A Historical Overview and Future Prospects." JAPANESE JOURNAL OF APPLIED PHYSICS PART 1 REGULAR PAPERS SHORT NOTES AND REVIEW PAPERS **44**(12): 8269.

Kudo, A. (2006). "Development of photocatalyst materials for water splitting." International Journal of Hydrogen Energy **31**(2): 197-202

Ni, M., et al. (2007). "A review and recent developments in photocatalytic water-splitting using for hydrogen production." Renewable and Sustainable Energy Reviews **11**(3): 401-425.

9. APPENDIX

Elemental Analysis with SEM.

The elemental analysis in SEM was done using *energy- dispersive x-ray spectroscopy* (EDS). This was done to approximate the different amounts/ratio of Ti to Nb. The results from the different specimens, and in some of them from different places/sites, are show in the diagrams below.

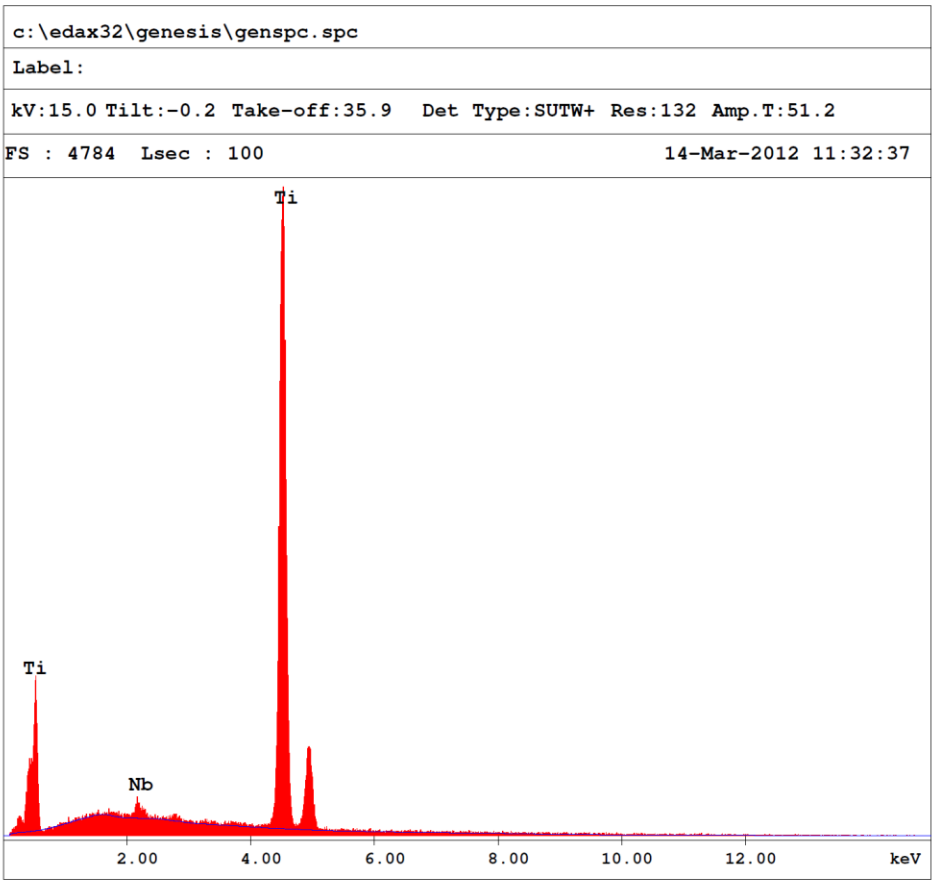

Element	Wt %	At %	K-Ratio	Z	A	F
NbL	2.25	1.17	0.0199	0.9069	0.9599	1.0138
TiK	97.75	98.83	0.9758	1.0020	0.9964	1.0000
Total	100.00	100.00				

Element	Net Inte.	Bkgd Inte.	Inte. Error	P/B
NbL	10.21	12.83	5.84	0.80
TiK	476.62	6.75	0.46	70.66

Figure 1: EDS graph of 1% doped (grain)

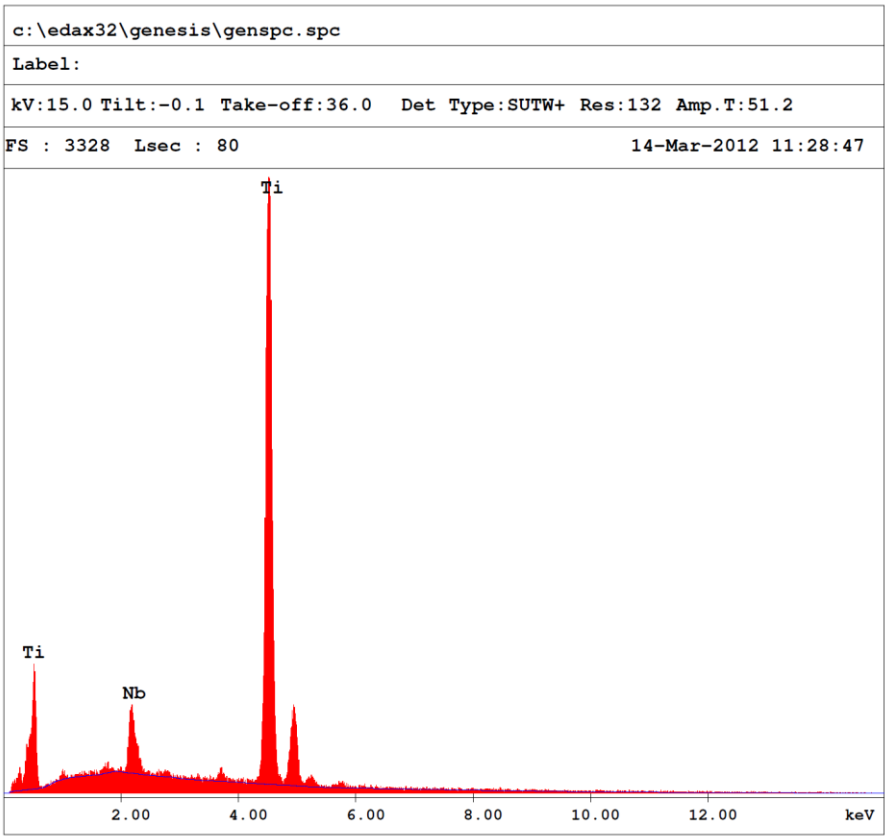

Element	Wt %	At %	K-Ratio	Z	A	F
NbL	8.47	4.55	0.0752	0.9118	0.9627	1.0118
TiK	91.53	95.45	0.9097	1.0074	0.9865	1.0000
Total	100.00	100.00				

Element	Net Inte.	Bkgd Inte.	Inte. Error	P/B
NbL	36.42	13.45	2.43	2.71
TiK	418.92	7.76	0.55	53.95

Figure 2: EDS graph of 1% doped (grain boundary)

The above results are taken from the EDS measurement of 1% Nb-doped TiO_2. Diagram 1 was taken from the grain of the material, whilst diagram 2 was taken from the lighter part situated in the grain boundary. From the results, it can be seen that the atomic percentage of Nb is greater in the lighter part of the grain boundary than in the grain. This results supports the micrograph from the BSE detector the SSD. Results from the grain show that the atomic percentage is close to 1%.

c:\edax32\genesis\genspc.spc

Label:

kV:20.0 Tilt:2.6 Take-off:37.1 Det Type:SUTW+ Res:132 Amp.T:102.4

FS : 4511 Lsec : 50 19-Apr-2012 20:48:10

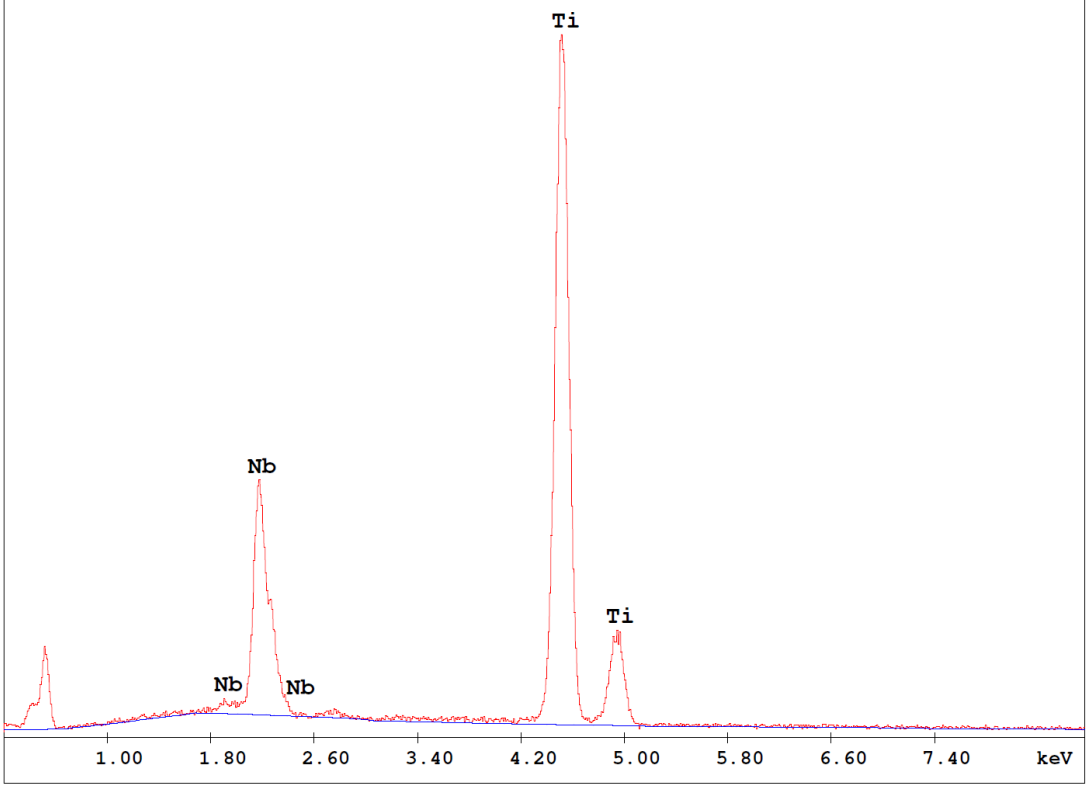

Element	Wt %	At %	K-Ratio	Z	A	F
NbL	26.58	15.73	0.2370	0.9291	0.9505	1.0099
TiK	73.42	84.27	0.6978	1.0195	0.9321	1.0000
Total	100.00	100.00				

Element	Net Inte.	Bkgd Inte.	Inte. Error	P/B
NbL	225.10	20.82	1.03	10.81
TiK	827.98	11.66	0.50	71.01

Figure 3: EDS graph of 30% doped (Supected rutile phase)

c:\edax32\genesis\genspc.spc

Label:

kV:20.0 Tilt:2.6 Take-off:37.1 Det Type:SUTW+ Res:132 Amp.T:102.4

FS : 4720 Lsec : 50 19-Apr-2012 21:02:38

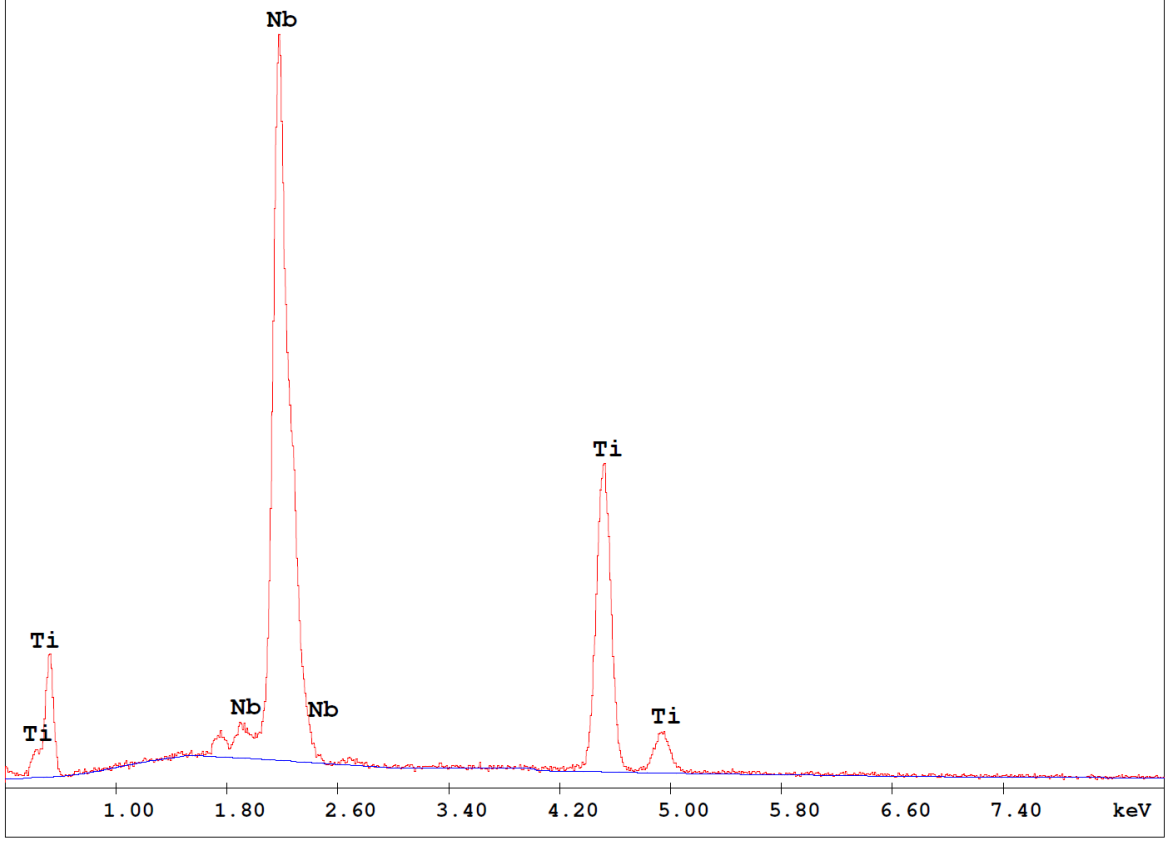

Element	Wt %	At %	K-Ratio	Z	A	F
NbL	68.66	53.04	0.6527	0.9672	0.9797	1.0031
TiK	31.34	46.96	0.2782	1.0545	0.8419	1.0000
Total	100.00	100.00				

Element	Net Inte.	Bkgd Inte.	Inte. Error	P/B
NbL	676.12	25.70	0.56	26.31
TiK	360.08	15.92	0.78	22.62

Figure 4: EDS graph of 30% doped (Suspected non rutile phase)